Palaeogeography, Palaeoclimatology, Palaeoecology 532 (2019) 109231

Contents lists available at ScienceDirect

Palaeogeography, Palaeoclimatology, Palaeoecology

journal homepage: www.elsevier.com/locate/palaeo

Tracking Holocene palaeostratification and productivity changes in the Western Irish Sea: A multi-proxy record

Mark A. Woods[a,*], Ian P. Wilkinson[a], Melanie J. Leng[b,c], James B. Riding[a], Christopher H. Vane[a], Raquel A. Lopes dos Santos[a], Sev Kender[a,g], Stijn De Schepper[d], Jan A.I. Hennissen[a], Sophie L. Ward[f], Charles J.B. Gowing[a], Philip R. Wilby[a], Matthew D. Nichols[e], Christopher A. Rochelle[a]

[a] British Geological Survey, Nottingham, UK
[b] Centre for Environmental Geochemistry, University of Nottingham, UK
[c] NERC Isotope Geosciences Laboratory, British Geological Survey, Nottingham, UK
[d] NORCE Climate, NORCE Norwegian Research Centre AS, Bjerknes Centre for Climate Research, Jahnebakken 5, 5007 Bergen, Norway
[e] Ocean and Earth Science, National Oceanography Centre Southampton, University of Southampton, UK
[f] Centre for Applied Marine Sciences, School of Ocean Sciences, Menai Bridge, Bangor University, UK
[g] Camborne School of Mines, University of Exeter, Penryn, Cornwall, UK

ARTICLE INFO

Keywords:
Microfossils
Stable isotopes
Rock-Eval
Sea surface temperature
Methane
Palaeotidal modelling

ABSTRACT

The Western Irish Sea preserves an exceptionally thick (ca. 40 m) Holocene succession that is ideally suited to understanding the pattern of palaeostratification and water mass productivity changes in the region, and their relationship with sea level, sedimentation, and biota. Additionally, the presence of shallow-buried methane provides an opportunity to explore its potential impact on the local pattern of Holocene marine environmental change. Multi-proxy investigation of a cored borehole succession through the Holocene interval tracks changes from mixed to seasonally stratified conditions. In the earliest Holocene (11.2–10 ka), high productivity, mixed water conditions prevailed, with abundant and diverse foraminifera and dominant heterotrophic dinoflagellate cysts. Productivity was probably driven by high nutrient fluxes related to high rates of sedimentation (> 1600 cm/kyr), in turn influenced by relatively low sea level and restricted sediment accommodation space across shelf areas to the east of the borehole site (eastern Irish Sea Basin). With rising sea level in the later part of the Early Holocene, the region evolved into a relatively lower productivity mixed water mass system, with significant changes in ecology revealed by dinoflagellate cysts and foraminifera. In the latest Early Holocene and earliest Mid Holocene (ca. 8.4–8.2 ka) a return to higher productivity is signalled by dinoflagellate cyst data; a result of seasonal stratification becoming established, evidenced by sharply increased summer sea surface temperature estimates (typically 16–17 °C) that contrast with an opposite (more positive) trend in $\delta^{18}O$ values for benthic foraminifera. Reductions in turbulent mixing associated with stratification might have exacerbated the palaeoecological impact of shallow-buried methane associated with the borehole site, potentially evidenced by a significant change in dominant benthic foraminifera and strong, localised excursions in the benthic $\delta^{13}C$/$\delta^{18}O$ record.

1. Introduction

Detailed evidence of relative sea level change in the Holocene has been assembled from an array of sites around the margin of the Irish Sea Basin, combined with modelling of glacial isostatic adjustment (GIA) response following the collapse of Late Devensian ice sheets (Lambeck, 1995; Lambeck and Purcell, 2001; Shennan and Horton, 2002; Roberts et al., 2006; Brooks et al., 2008; Bradley et al., 2011; Smith et al., 2012). Yet little is known about the pattern of Holocene environmental change in deeper parts of this basin; a region that hosts shallow-buried methane and related gas-escape structures (Crocker et al., 2005; Judd, 2005; Fig. 1), and where localised seasonal water-mass stratification is important for marine productivity today (Gowen et al., 1998).

Seasonal water-mass stratification currently develops in an isolated part of the Western Irish Sea (WIS), where tides entering from the south (St George's Channel) and from the north (North Channel) meet to

* Corresponding author.
E-mail address: maw@bgs.ac.uk (M.A. Woods).

https://doi.org/10.1016/j.palaeo.2019.06.004
Received 4 March 2019; Received in revised form 31 May 2019; Accepted 3 June 2019
Available online 06 June 2019

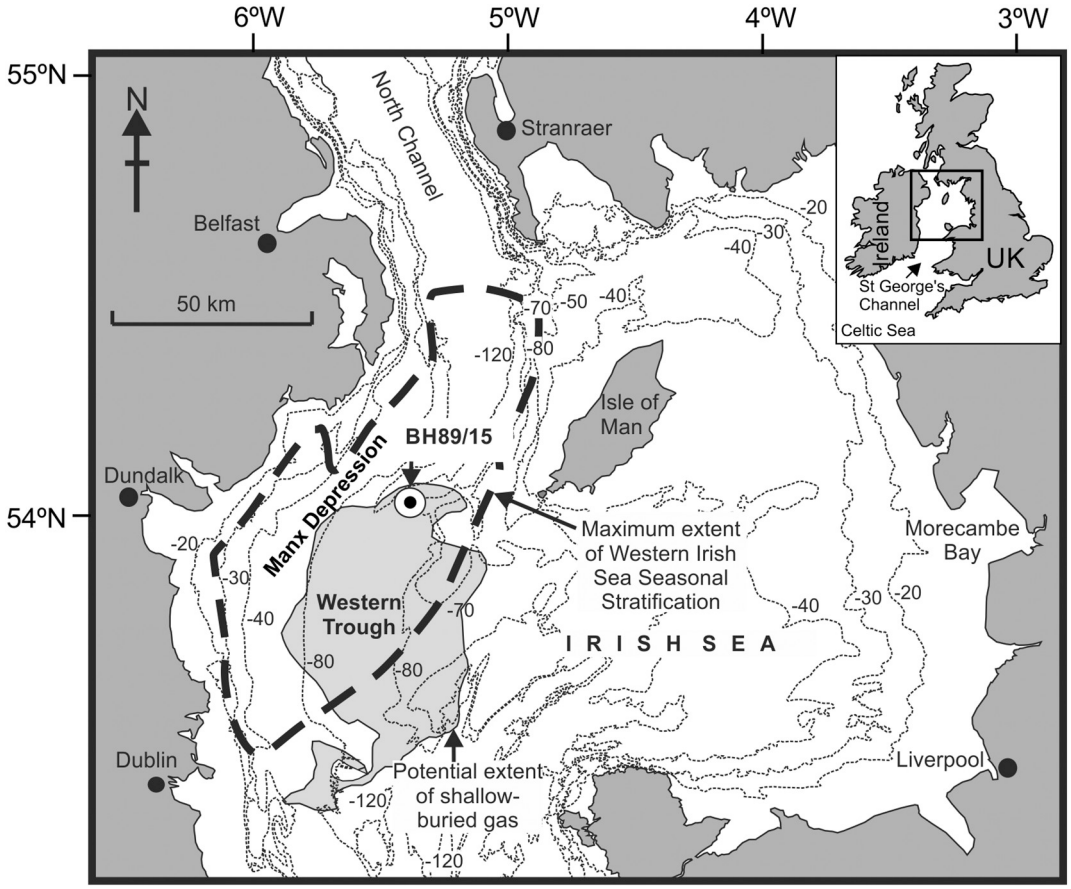

Fig. 1. Geography and bathymetry of the Irish Sea, showing location of Borehole 89/15 and approximate extents of present-day seasonal water mass stratification and shallow-buried gas deposits in the Western Irish Sea. Bathymetry (in metres) from DigBath250 digital data (British Geological Survey © NERC). Derived in part from data provided by Vlaamse Hydrografie (Belgium), Bundesamt för Seeschifffahrt und Hydrographie (BSH - Germany), Bureau Hydrografie (Netherlands), Statens Kartverk (Norway), Farvandsvæsenet (Denmark) and United Kingdom Hydrographic Office. Stratification extent based on Howarth (2005) and gas data based on Crocker et al. (2005).

create a region of permanent slack water south-west of the Isle of Man (Dabrowski et al., 2010; Fig. 1). In late spring and summer, weak tidal mixing combines with reduced wind shear and increased solar insolation, allowing thermal/density stratification to develop (Hill et al., 1996; Howarth, 2005; Dabrowski et al., 2010; Williams et al., 2013). Short-lived phytoplankton blooms develop in near-surface waters across the stratified region in the spring, exploiting enhanced water clarity and consuming nutrient residues stirred up by the winter storms (Sharples et al., 2010). At the margins of the stratified water mass, deeper water nutrient flows are concentrated at mixing fronts, boosting marine productivity in these regions (Austin and Scourse, 1997; Sharples, 2008). Nutrients are also harvested by a narrow, concentrated band of phytoplankton (Sub Chlorophyll Maximum) developed at the density gradient (pycnocline) between warm (near-surface) and cool (deeper) water masses across stratified regions, sustaining organic fluxes to the seabed and depressing dissolved oxygen concentrations (Scourse et al., 2002; Greenwood et al., 2010; Sharples et al., 2010; Williams et al., 2013). These processes underpin economically important marine fisheries (e.g. Hill et al., 1996), and more generally disproportionately boost the contribution of shelf seas to total global oceanic primary production (15–30%; Wollast, 1998) and the marine storage of carbon dioxide (20–50%) through the mechanism referred to as the 'shelf sea pump' (Rippeth, 2005).

Here we present a multidisciplinary study of a thick (ca. 40 m) Holocene cored borehole succession in the WIS (Fig. 1), located within the region of present-day seasonal water-mass stratification and shallow-buried methane. The borehole is ideally positioned to explore the impact of sea-level change on the deep marine shelf, and to reveal the Holocene record of changes in water-mass productivity in an unusually expanded succession compared to that previously reported in the Celtic Sea (Austin and Scourse, 1997; Scourse et al., 2002). The potential influence of changes in water-column circulation on methane accumulation and seepage at the borehole site (Judd, 2005), and the extent to which this has impacted the marine ecology of the region, are significant further objectives of this work.

2. Material and previous research

The borehole (BGS index 89/15; 54.0360^{0}N, 5.3458^{0}W), drilled in 1989 to a total depth of 85 m, is located in a narrow deep water region in the central part of the WIS forming part of the Manx Depression. Southwards this region forms the Western Trough, between 80 and 120 m water depth, whilst northwards there is further deepening (below 140 m) into the North Channel, linking the Irish Sea with the Atlantic (Fig. 1). The cored succession comprises 39.3 m of Holocene sediments, unconformably overlying 45.7 m of Pleistocene deposits (including at 40.05–44.15 m depth foraminifera, ostracods and dinoflagellate cysts indicative of cold Late Devensian climate conditions; Riding, 1995; Wilkinson, 1995; Dickson, 1995), collectively forming part of the Western Irish Sea Formation (Chesher and Wingfield, 1990; Jackson et al., 1995). The Holocene strata, predominantly comprise pale grey-coloured clay and silty clay, becoming increasingly micaceous below 20 m, with shell and sand-rich intervals towards the base of the succession (Fig. 2A). A sharp erosional contact and pebble bed occurs at

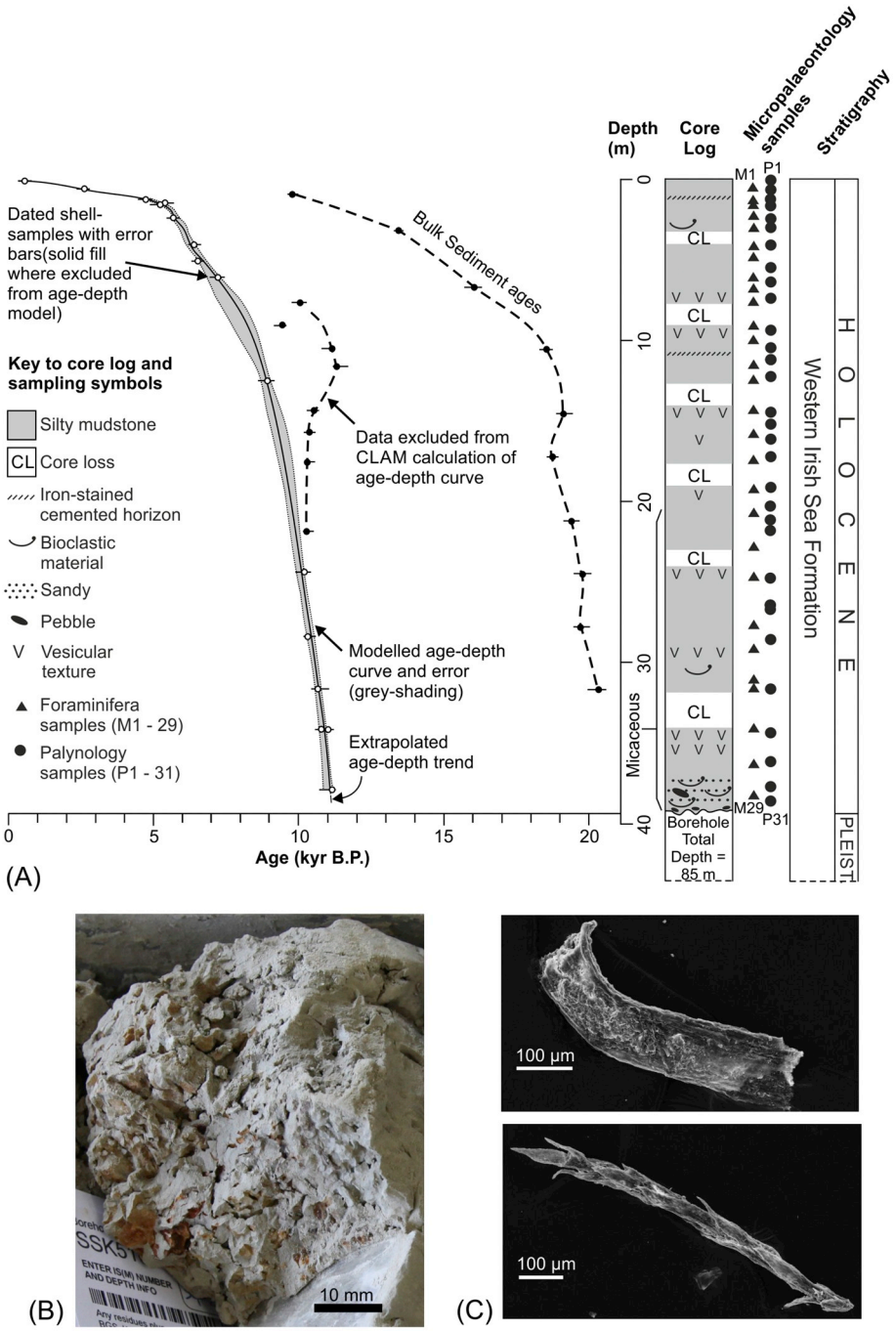

Fig. 2. (A) Stratigraphy, borehole core log, micro-fossil sampling and age-depth model for Borehole 89/15. Age-depth model (solid line) calculated from CLAM 2.2 (Blaauw, 2010) using calibrated radiocarbon ages for samples of shell material. (B) Image of 'vesicular texture' representing core intervals that were methane-bearing when drilled. (C) SEM images of woody plant fragments in Holocene sediment residues from Borehole 89/15. This 'old' carbon helps explain the relatively greater ^{14}C age of the bulk sediment compared to that determined for individual foraminifera. Scale bar = 10 mm; Pleist = Pleistocene.

39.3 m, marking the base of the Holocene (Wilkinson, 1995) and a rapid downward transition to pale red-coloured glaciomarine sediments (Chesher and Wingfield, 1990). Below the Quaternary succession at the borehole site, regional geophysical data indicate the presence of a thick (+1000 m) succession of Permo-Triassic rocks occupying a structurally complex fault-bounded basin (Peel Basin) west and southwest of the Isle of Man (Chadwick et al., 2001). Apart from limited sampling of the core to establish broad biostratigraphical and palaeoecological interpretations (Dickson, 1995; Riding, 1995; Wilkinson, 1995), and reference to the presence of shallow-buried methane at the borehole site (Judd, 2005), no detailed work has been carried out on this uniquely thick Irish Sea Holocene succession.

References to subdivisions of the Holocene (Early/Mid/Late) follow Walker et al. (2012, 2018). All borehole depths are metres below top of core. All ages reported in this article are calibrated radiocarbon years (cal BP). Author citations for taxa follow the Ellis and Messina Catalogue of Foraminifera (ISBN 978-0-913424-34-6), and Williams et al. (2017) for dinoflagellate cysts.

3. Methodology

For this study we focus on the Holocene succession, integrating a

^{14}C age/depth model with a range of environmental proxies to track changes in marine mixing ($U^{K'}_{37}$, δ^{13}C, δ^{18}O), water mass productivity (foraminifera, dinoflagellate cysts, Rock-Eval) and sediment characteristics (XRFS).

The stratigraphical distributions and relative abundances of foraminifera (M1–29; Fig. 2A) and dinoflagellate cysts (P1–31; Fig. 2A) were analysed in the upper 39.3 m of the core. Calcareous micropalaeontology samples were prepared from air-dried residues of core samples washed through a 63 μm sieve with de-ionised water, and taxa counts based on the 125–1000 μm size fraction. Slides for palynological analysis were prepared using a standard processing technique (Wood et al., 1996). Systematic abundance counts were made for all the samples, with correspondence analysis used to explore their taxonomic similarity.

Bulk sediment geochemistry was measured for 204 samples using a portable Niton XLt 793 X-Ray Fluorescence Spectrometer (XRFS), fitted with a 40 kV Ag anode X-ray tube. Samples were milled to < 32 μm powders using agate planetary ball mills and analysed for 120 s using the XRFS in a static semi-automated configuration with 'Standard Soil Mode' selected. A subset of 13 samples was selected for laboratory XRFS analysis (using PANalytical Axios sequential, wavelength-dispersive X-ray fluorescence spectrometer, fitted with a 60 kV generator and 4 kW rhodium (Super Sharp) end–window X-ray tube) to permit data calibration.

The type, quantity and maturity of sedimentary organic matter, and its variation through the succession, was assessed by Rock-Eval pyrolysis using a Rock-Eval 6 analyser configured in standard mode (pyrolysis and oxidation as a serial process) following the methodology of Slowakiewicz et al. (2015). Rock-Eval parameters were calculated by integration of the amounts of HC (thermally-vaporized free hydrocarbons) expressed in mgHC/g rock (S1) and hydrocarbons released from cracking of bound organic matter (OM) expressed in mgHC/g rock (S2). The Hydrogen Index (HI) was calculated from S2 × 100/Total Organic Carbon (TOC) and the Oxygen Index (OI) from S3 × 100/TOC.

Age data were obtained by ^{14}C analysis of 35 samples of mixed shell material (samples individually comprising either echinoderm or mollusc shell, or ostracods and foraminifera, or a combination of these components), between the top of the core and 37.9 m depth, using the Natural Environment Research Council (NERC) Radiocarbon Facility (East Kilbride) and the Keck C Cycle AMS Laboratory, University of California (Irvine). A preliminary set of 10 bulk sediment radiocarbon ages was used to guide borehole sampling. These bulk samples showed that the 0–20 m core interval age range is much greater than the 20–37.9 m interval, and sample frequency, for both detailed age (^{14}C) – depth modelling and other analyses, was adjusted accordingly. Monospecific dating of shell samples was not attempted because sample weights were consistently below the critical weight for accurate age determination, even when the depth ranges of samples was increased. Although use of mixed shell material may potentially lead to lower age precision because of different ecological factors associated with different taxa, analysis of archaeological samples has shown that for molluscs at least, ^{14}C measurements from a range of taxa sampled from well-constrained horizons show no significant age variation (Ascough et al., 2005). Other work (Heier-Nielsen et al., 1995; Barker et al., 2007) suggests that our inclusion of marine macrofossil shell for dating may have significant advantages for age reliability compared to dates based on foraminifera alone. In all cases, pristine shell material was selected to reduce potential error caused by reworking.

Calibrated radiocarbon (^{14}C) ages for shell samples were converted into an age-depth profile using CLAM (Version 2.2) (Blaauw, 2010; http://chrono.qub.ac.uk/blaauw/clam.html) using the Intcal calibration curve and applying an average reservoir correction of −62 ^{14}C yrs (Butler et al., 2009). No correction was made for methane, which is probably thermogenic in the WIS (Crocker, 1995) with negligible radiogenic carbon (Winckler et al., 2002). Nor are age data likely to be significantly compromised by the dead carbon content of methane, based on recent data from cold seep sites in Japan (Yagasaki et al., 2016).

Age/depth reversals shown by preliminary results are evident in replicate analyses and bulk samples, suggesting they are real features of the succession and not sampling/analytical errors. The age reversals are associated with an interval of the borehole containing units of core loss (Fig. 2A) and most of the units of core loss are associated with units of vesicular textured sediment above or below them (Fig. 2A, B). This texture is probably associated with methane-rich intervals in the borehole succession, noted by Judd (2005) as occurring in Borehole 89/15 at depths down to 36 m. High gas content is likely to have reduced sediment cohesion during drilling, causing local collapse as confining pressure is reduced, or allowing sediment to become entrained in the circulating drilling lubricant or mixed with adjacent sediment. The archive copy of the borehole log at 31–32 m depth, just above an interval of core loss, records additional drilling weight required to compensate for gas back-pressure.

To mitigate the effects of age reversals on age-depth modelling, selection of the most reliable data points for detailed model calculation (Fig. 2A) was guided by the general trend of bulk sediment age data, ignoring the age-reversals. This trend closely matches that of dated shell material, but is consistently older, probably indicating significant 'dead' carbon (Fig. 2C) fed from the source areas for Holocene sediment. In our Rock-Eval data, this is represented by values for non-pyrolisable carbon (RC (%)), which locally exceeds 90% of TOC in the lower part of the borehole, and remains > 70% near the top of the succession.

A further series of 210 samples of the two long-ranging and numerically dominant benthonic foraminifera *Quinqueloculina seminula* and *Ammonia beccarii* provided calcite for stable isotope analysis (δ^{13}C, δ^{18}O), with representative specimens from a range of depths assessed for diagenetic alteration using SEM imagery (BSEM and EDX) and optical cathodoluminescence (CL). In the context of the previously recorded presence of shallow-buried methane at the study site (Judd, 2005), and the potential of this to produce methane derived authigenic carbonate (MDAC), CL analysis was considered a useful cross-check on the extent of any diagenetic alteration that might not immediately be apparent from visual observations. Isotope analyses were performed at BGS with an Isoprime dual inlet mass spectrometer plus Multiprep device, using 30–100 μg of calcite. Isotope values (δ^{13}C, δ^{18}O) are reported as per mille (‰) deviations of the isotopic ratios (^{13}C/^{12}C, ^{18}O/^{16}O) calculated to the VPDB scale using a within-run laboratory standard calibrated against NBS-19 (δ^{13}C = +1.95‰ and δ^{18}O = −2.20‰ as defined by IAEA). Analytical reproducibility of the standard Carrara marble (δ^{13}C = +2.00‰ and δ^{18}O = −1.73‰) is 0.03‰ for δ^{13}C and 0.06‰ for δ^{18}O (n = 27). Craig correction is also applied to account for ^{17}O (Craig, 1957).

Finally, alkenone-based estimates of Holocene sea surface temperatures (SSTs) were calculated for 26 sediment samples spanning the Holocene interval based on lipids extracted using an accelerated solvent extractor (ASE 200, Dionex) and gas chromatography analysis (Hewlett Packard 6890 equipped with flame ionization detection (FID) and an Agilent DB-1 ms UI column). $U^{K'}_{37}$ values were calculated using the equation of Prahl and Wakeham (1987), and SST values estimated using the global core top calibration of Müller et al. (1998).

4. Results

All raw and calibrated data relating to this study are provided as a data appendix, and also deposited at the National Geoscience Data Centre, British Geological Survey, Keyworth, Nottingham (DOI: https://doi.org/10.5285/d959d29f-7660-4acc-82e2-2ef2203adb70), where all core and sample materials can be examined.

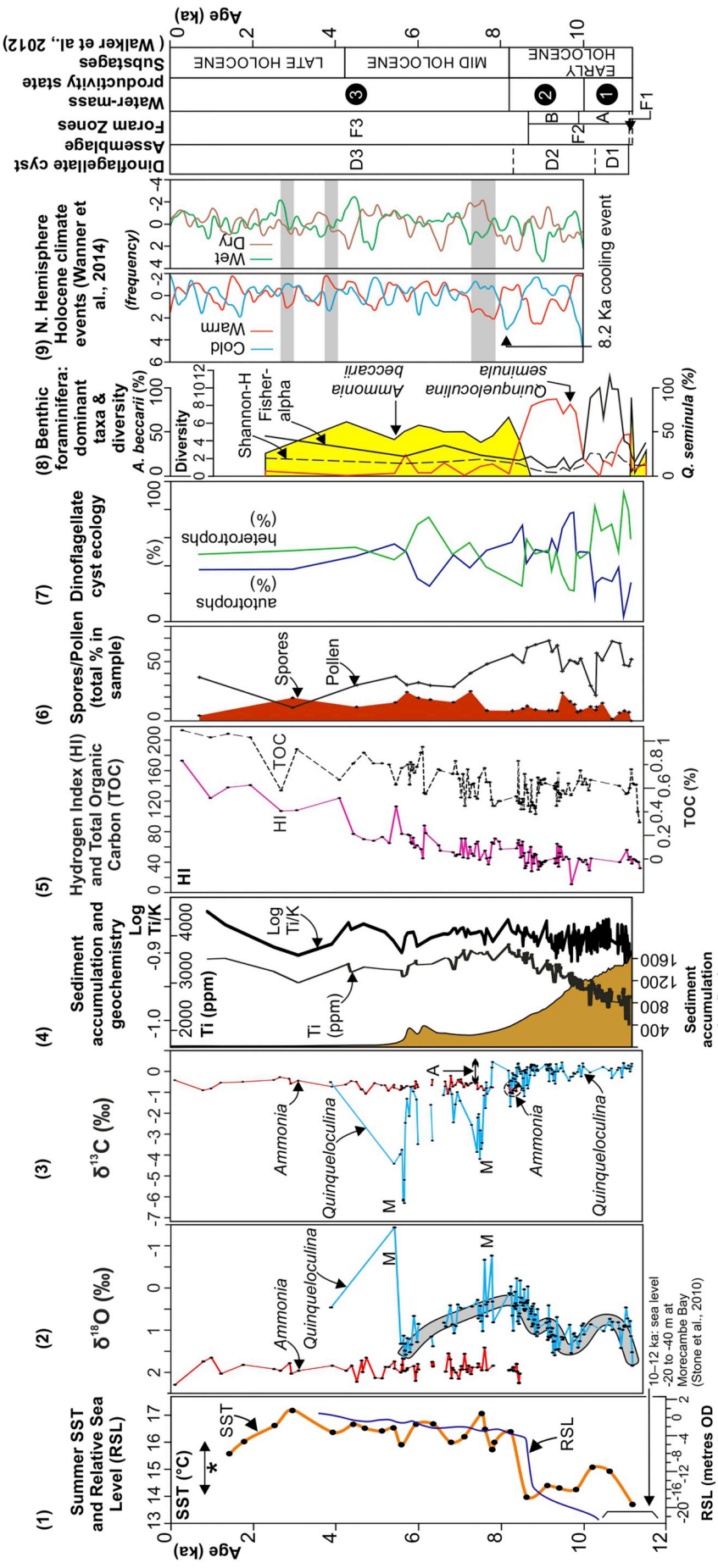

Fig. 3. Comparison of selected data for the Holocene succession in Borehole 89/15 plotted against age and interpretations of biostratigraphical (dinoflagellate cysts, foraminifera) and palaeoecological subdivisions. (1) Relative sea level data for Morecambe Bay UK (Smith et al., 2012, fig. 1) and summer SST (* = typical current summer SST) range for Irish Sea measured at Cypris Station, Isle of Man between 1904 and 2004 (Evans et al., 2003); (2) $\delta^{18}O$ for benthic foraminifera (*Quinqueloculina*, *Ammonia*) with general trends highlighted by grey shading. Aberrant peaks labelled 'M' may indicate the influence of seafloor methane seepage on isotope values; (3) $\delta^{13}C$ for benthic foraminifera (*Quinqueloculina*, *Ammonia*), with peaks ('M') potentially influenced by seafloor methane seepage. Difference between maximum $\delta^{13}C$ for *Quinqueloculina* before and after stratification indicated by 'A'; (4) Sediment accumulation compared with total concentration of Ti and Log Ti/K; (5) Hydrogen index (HI) compared with Total Organic Carbon (TOC) determined from Rock-Eval analysis; (6) Percentage spores and pollen; (7) Percentage autotrophic and heterotrophic dinoflagellate cysts; (8) Foraminifera diversity and abundance distribution of *Quinqueloculina* and *Ammonia*; (9) Frequency of warm/cold and wet/dry Holocene climate events of Wanner et al. (2014), with grey highlight indicating events that align with SST inflections.
Water mass productivity state: 1 = Mixed marine, high productivity; 2 = Mixed marine, low productivity; 3 = Seasonally stratified, high productivity.

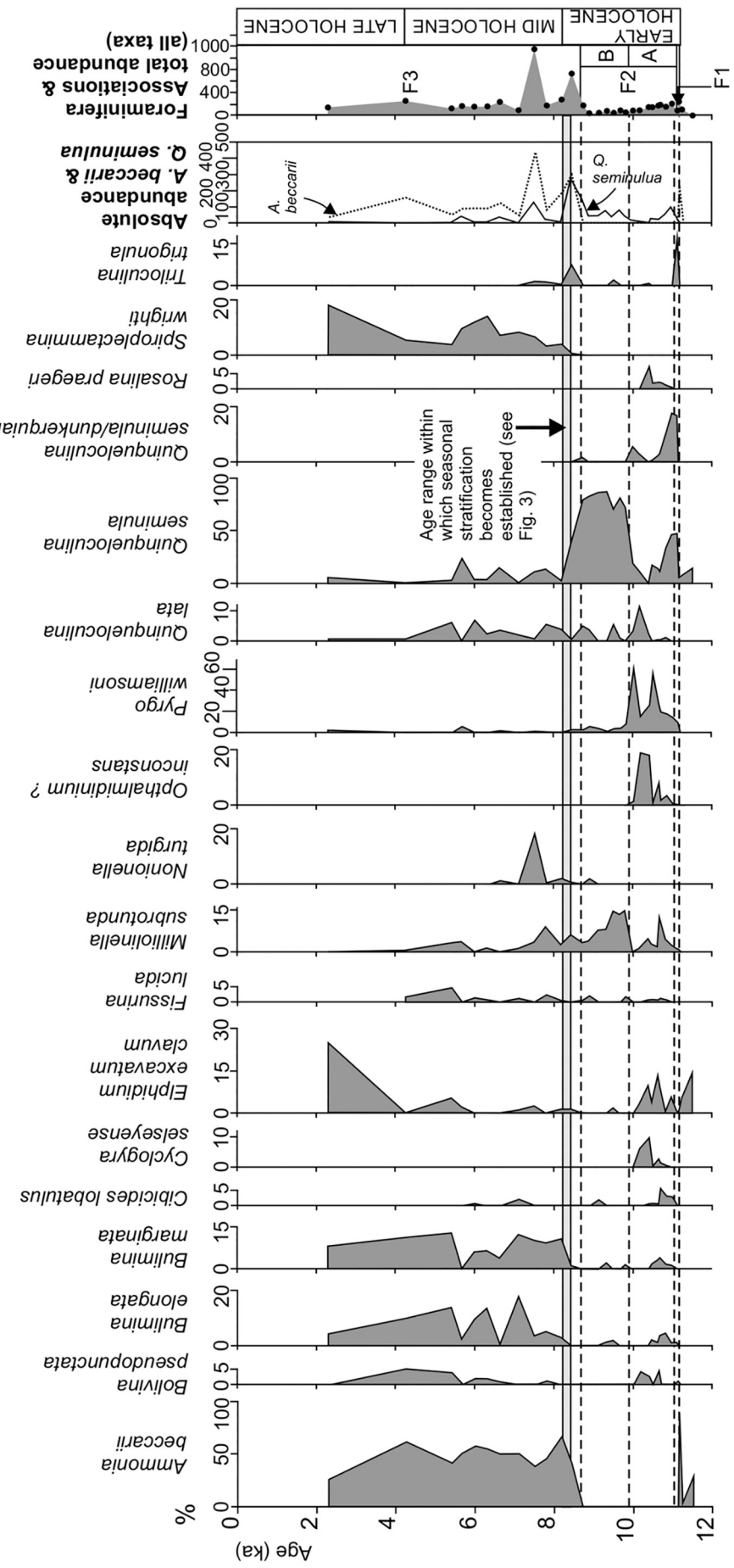

Fig. 4. Relative abundance of selected foraminifera in the Holocene succession of Borehole 89/15 with respect to subdivisions based on foraminifera associations, total foraminifera diversity, total foraminifera abundance and onset of seasonal stratification. Excludes taxa where the sum of percentage abundances in all samples is low (< 15%). The numerical dominance of *Quinqueloculina* in most Early Holocene assemblages is rapidly replaced by *Ammonia*, *Bulimina* and *Spiroplectammina* in the Mid and Late Holocene. A complete listing of all the foraminifera taxa identified in the samples, and their raw abundances, is provided in Supplementary Data.

4.1. Radiocarbon (^{14}C) dating

The best-fit age-depth model shows very high rates of sedimentation in the lower part of the borehole (below 12 m), rapidly declining upwards, particularly above 2 m depth (Fig. 2A). Ages for small intervals of the borehole (highest 0.05 m and lowest 1.4 m) not covered by the age-depth model are derived by extrapolation from the immediately adjacent age-depth trends. This suggests an age of ca. 11.2 ka for the unconformity surface inferred to mark the base of the Holocene at 39.3 m.

4.2. Foraminifera

The Holocene succession contains three stratigraphically distinct foraminiferal associations (F1 to F3; Fig. 3) that allow subdivision as follows (Fig. 4):

F1: *Ammonia beccarii* association (39–39.1 m; ca. 11.17 ka): Flood abundance of *A. beccarii* and subordinate *Quinqueloculina seminula*.
F2: *Quinqueloculina seminula – Pyrgo williamsoni* association (11.6 m–38.3 m; 8.7–11.1 ka): Dominated by miliolid taxa and "species of southern origin" sensu Murray (1971, 1973, 1991) including *Rosalina praegeri*, *Bulimina elongata*, *B. marginata*, *Asterigerina mamillata* and *Bolivina pseudoplicata*. Rare *Virgulina* (=*Stainforthia* of Scott et al., 2003).
F3: *Spiroplectammina wrighti* - *A. beccarii* association (0–10.56 m; 0–8.5 ka): Numerically dominated by *A. beccarii*, but uniquely characterised by *S. wrighti*. This assemblage is also characterised by agglutinated taxa including *Textularia sagittula*. *Bulimina* is more numerous and consistent in its occurrence compared to underlying units, with peak abundance at 6.88–6.95 m (ca.7.5 ka).

Correspondence analysis of the foraminifer assemblages (Fig. 5) reveals that samples belonging to F2 and F3 define clusters of points, and that F2 can be subdivided into a more diverse lower part (F2a; ca. 38.3–21.2 m, 11.1–9.9 ka), and an upper part (F2b; ca. 21.2–10.56 m, 9.9–8.7 ka) with markedly reduced diversity resulting from a loss of hyaline taxa. Sample M28 is closely associated with points defining F2b, but is unrelated stratigraphically, occurring close to the base of the Holocene. The unusual low diversity of this sample may be influenced by rapidly transitioning Early Holocene environmental conditions. Sample M29 stratigraphically defines F1, but plots with points defining F3. This reflects the high abundance of *Ammonia* in this Early Holocene sample.

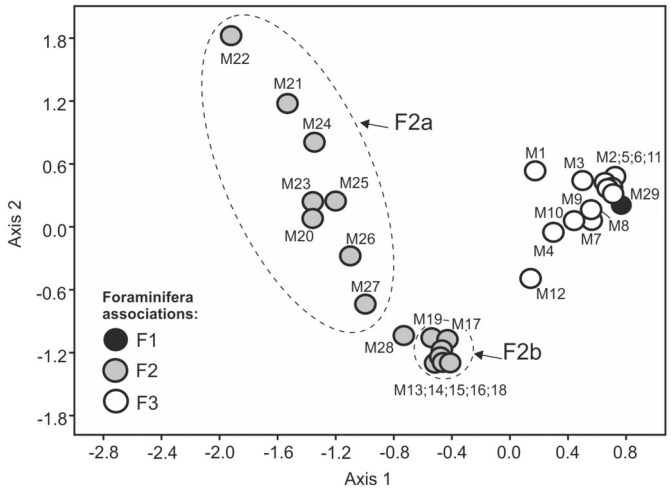

Fig. 5. Correspondence analysis of foraminifera samples (M1 (youngest) - M29 (oldest)) shaded to show relationship to stratigraphically constrained associations (F1, F2 & F3). The analysis allows subdivision of F2 into an early high diversity part (F2a) and a later low diversity interval (F2b). M28 and M29 have unusual taxonomic features (probably influenced by Early Holocene environmental conditions) that distort their positions on this plot (see text for details). DCA sample scores and eigenvalues are detailed in Supplementary Data.

With the exception of the occurrence of *Ammonia* in F1, one of the most striking features in Borehole 89/15 is the general dominance of *Quinqueloculina seminula* in the older parts of the succession (ca. 11–8 ka) and *Ammonia beccarii* in the younger part (post 8 ka) (Figs. 3 and 4).

4.3. Palynology

Three broad assemblages can be recognised in the stratigraphical distribution of dinoflagellate cysts (Fig. 6). The oldest (D1; 38.69–26.66 m; ca. 11.15–10.3 ka) assemblage is dominated by heterotrophic cysts (e.g. *Brigantedinium*), with relatively low proportions of *Spiniferites* and no *Operculodinium centrocarpum*. *Lingulodinium machaerophorum* is abundant in one sample (ca. 10.5 ka). Above this, assemblage D2 (26.41–9.27 m; ca. 10.3–8.3 ka) contains a higher number of taxa, with a higher and frequently dominant proportion of autotrophic taxa, including significant increases in the relative abundance of the genus *Spiniferites*. Also *Operculodinium centrocarpum* sensu Wall and Dale (1966), *Selenopemphix nephroides* and *Spiniferites membranaceus* appear in the record from around 10.3 ka. The youngest (D3; 7.29–0.07 m; ca. 7.7–0.6 ka) assemblage sees a return of a higher proportion of heterotrophic taxa (particularly *Brigantedinium*) that become dominant over autotrophic taxa. With the exception of a single occurrence in D2, *Bitectatodinium tepikiense* is only recorded in the D3 assemblage. There is also a gradual shift to higher average cyst concentrations in the younger sediments.

Detrended correspondence analysis (Fig. 7) reveals a strong distinction between samples comprising the D1 and D2 assemblages. The D3 assemblage occupies an intermediate region of the DCA plot, with the youngest samples from D3 showing increased similarity with D1.

4.4. Bulk geochemistry

Laboratory-calibrated bulk sediment XRFS analyses of selected elements (K, Ca, Ti, Fe, Rb, Sr) are plotted in Fig. 8, with element concentrations also presented as log ratios normalised to K (a proxy for clay in the absence of data for Al).

Plots of absolute and normalised Ca and Sr are very similar and show strong shifts in their relative concentration; high values at and near the base of the succession decline sharply towards 8 ka, and then increase progressively and more gradually above this to 3.1 ka. Sediment residues prepared for microfossil extraction suggest that the main contributors to the Ca and Sr plots are biogenic shell material and locally voluminous crystalline gypsum (Fig. 8), occurring as euhedral twinned crystals and inter-grown crystal rosettes. This gypsum does not have the typical crystal habit of 'gypsum spotting' that develops during storage and drying of borehole core. SEM analysis reveals clear signs of multi-stage growth of gypsum crystals (J C Rushton, BGS, pers. comm., 2015), and preliminary Sulphur isotope analysis ($\delta\ ^{34}S$) indicates a significant contrast with modern seawater, and suggests the potential for a pre-Holocene source (T E Heaton, BGS, pers. comm., 2015) or growth from sulphide oxidation. Sulphide oxidation could include in-situ alteration of pyrite, but the observation of pristine pyrite enclosed in gypsum crystals makes this origin seem unlikely, potentially favouring a relationship with shallow-buried methane and associated hydrogen sulphide (recorded on borehole drill logs).

Both Fe and K have a strong correlation with Ti ($R^2 = 0.88$ for Fe and 0.94 for K), and all have similar overall trends, with well-defined and coincident maxima around 8 ka. These similar trends suggest a common link to sediment input, with the Fe predominantly in the form of oxy-hydroxide rich particulates. The trend in Ti concentration is approximately inverse to those of Ca and Sr, and also to sediment

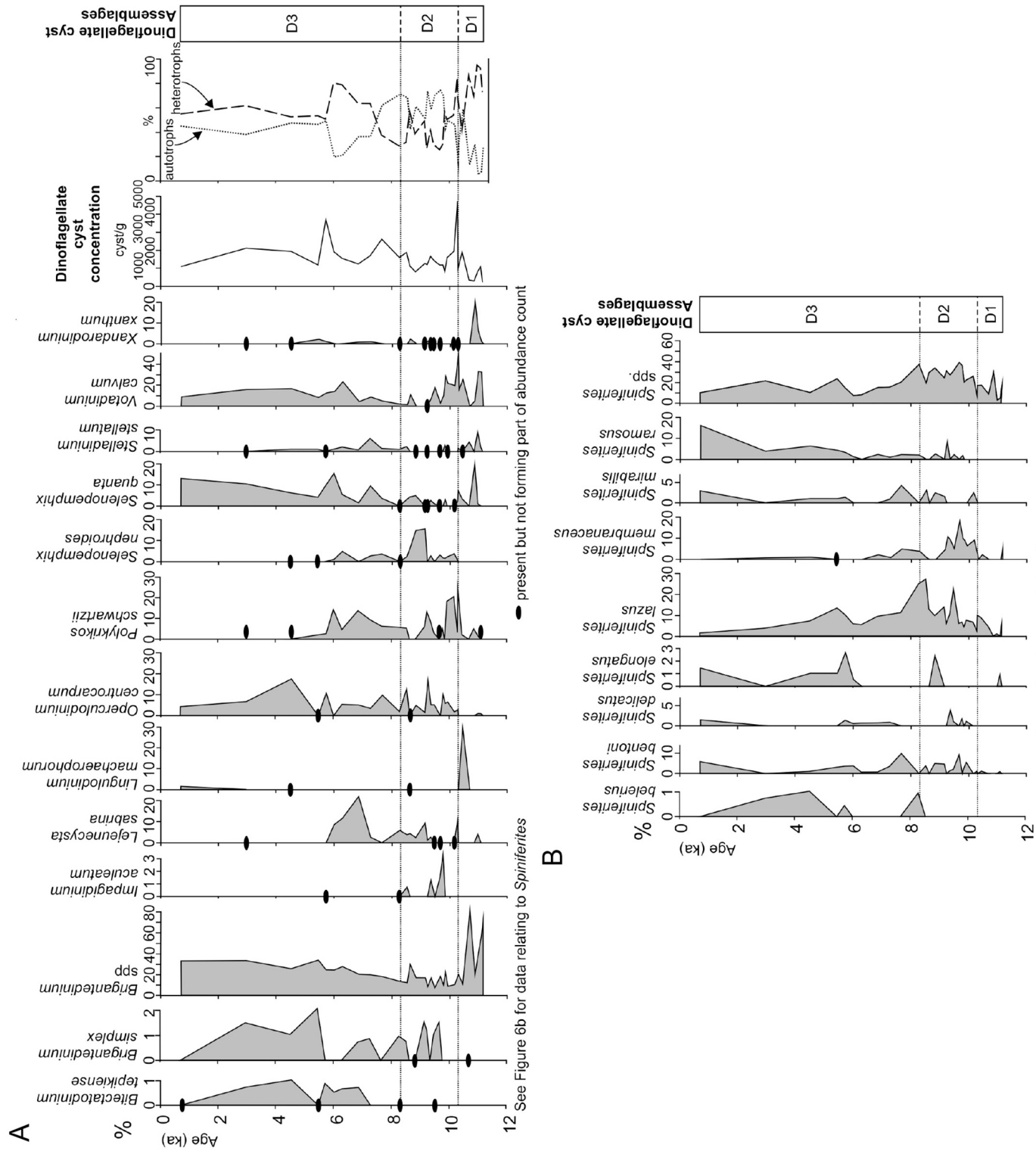

Fig. 6. Relative abundances of selected dinoflagellate cyst taxa for the Holocene succession of Borehole 89/15, and its subdivision based on dinoflagellate cyst assemblages. P = Peridinalid taxa, G = Gonyaulacid taxa. 6A: Relative abundances of taxa excluding *Spiniferites*; 6B: Relative abundances of species of *Spiniferites*. Heterotrophic taxa dominate in D1, reduce in their relative proportion in D2, and show progressive increase and return to dominance in D3.

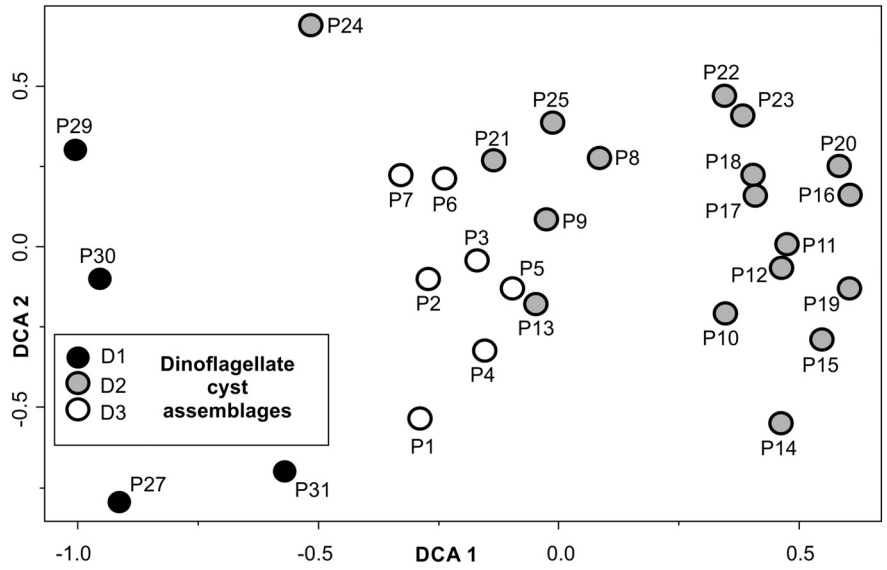

Fig. 7. Correspondence analysis of dinoflagellate cyst samples. Analysis excludes samples P24 and P26 which both have low cyst counts and have dominant occurrences of single taxa (*Lingulodinium machaerophorum* in P24 and *Xandarodinium xanthum* in P26). The plot shows a strong distinction between the D1 and D2 assemblages, with the D3 assemblage occupying an intermediate position. Younger parts of the D3 assemblage appear to show a trend of increasing similarity with the D1 assemblage (indicative of high productivity). DCA sample scores and eigenvalues are detailed in Supplementary Data.

accumulation rate prior to 8 ka. This somewhat counter-intuitive relationship is probably a dilution effect, largely driven by high concentrations of gypsum judging by records of sample residues (Fig. 8). In contrast, the normalised plot of Ti reveals peak values below 10 ka, and only modest changes in overall values at 10–8 ka (Fig. 8). Sharp peaks in the plots of total and normalised concentrations of Fe, occurring around 8.6 ka and 4.4 ka, correspond to thin, highly cemented, iron-stained horizons in the core (Fig. 8), and it is noticeable that unlike Ti, the normalised Fe plot shows a trend to lower values below 8 ka. In combination, these characteristics suggest that Fe concentration is somewhat independent of the dilution effects, and reflects its susceptibility to remobilisation in the sediment in response to changes in redox conditions.

4.5. Stable isotope composition ($\delta^{13}C$, $\delta^{18}O$)

The plot of $\delta^{18}O$ (Fig. 3) shows a strongly fluctuating pattern for *Quinqueloculina*, with the bulk of the data ranging between −0.25‰ and +1.5‰. There are two points on the curve where values for $\delta^{18}O$ are significantly more negative ('M' on Fig. 3), where values for

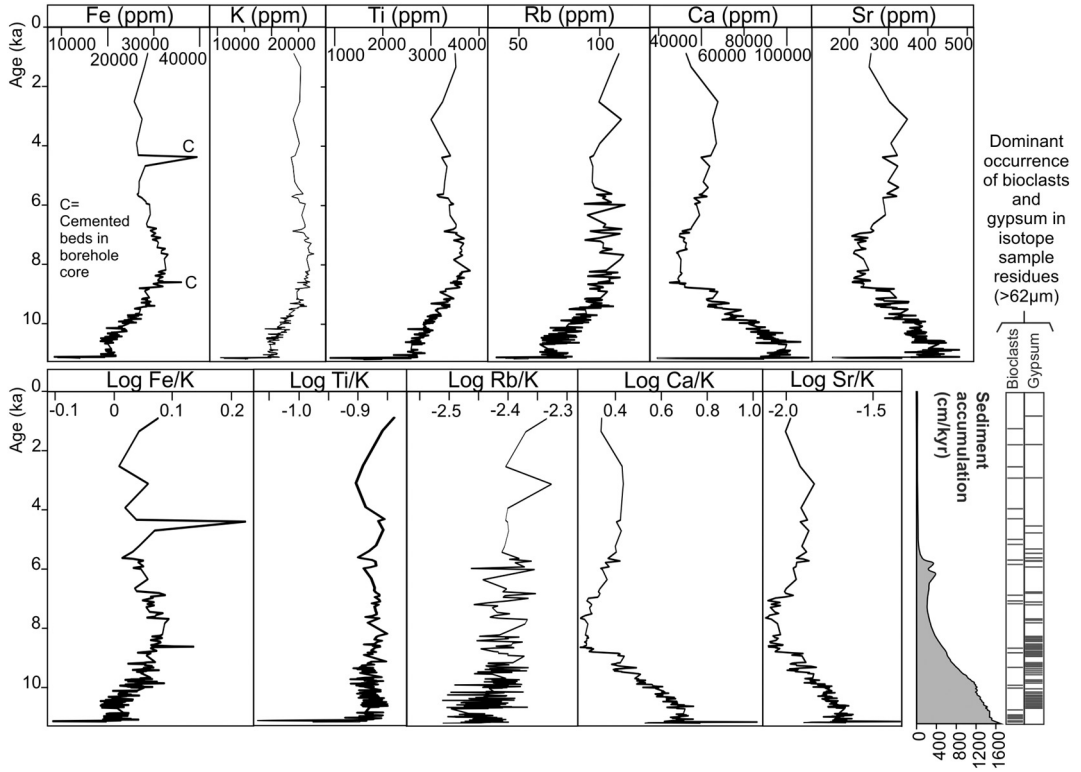

Fig. 8. Total concentration (ppm) and log ratio plots (normalised to K) of selected elements based on laboratory calibrated bulk sediment XRFS analysis of 204 samples from the Holocene succession in Borehole 89/15. Log ratio plots are normalised to potassium (K) and compared with sedimentation rate and composition of sediment residues prepared for stable isotope analysis. Plots of Fe, K, Ti and Rb predominantly record the type and quantity of sediment, although sharp peaks in Fe around 8.6 ka and 4.4 ka may be a response to local changes in redox state related to changes in seafloor methane seepage. Ca and Sr predominantly respond to the amount of bioclastic shell and gypsum in the succession, with the latter probably being the dominant influence in the lower part of the succession.

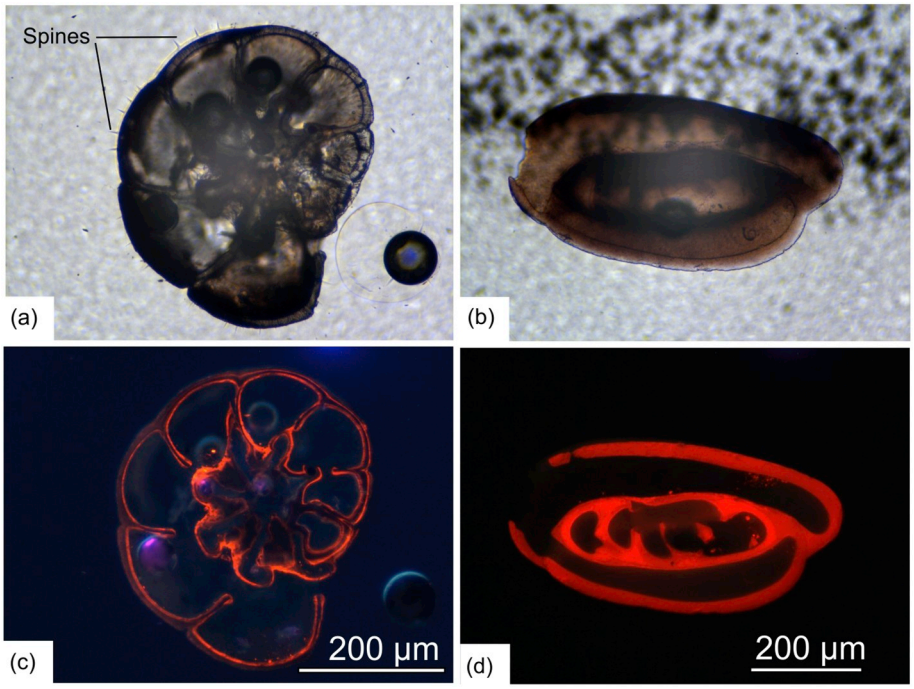

Fig. 9. Transmitted light SEM and CL imagery of polished thin sections of *Ammonia beccarii* (a, c) and *Quinqueloculina seminula* (b, d). The imagery shows good preservation of *Ammonia* (including spines) and *Quinqueloculina*, but luminescence of CL images suggests varying degrees of diagenetic alteration.

Quinqueloculina are between −0.5 and −1.5‰. The $\delta^{18}O$ plot for *Ammonia* is much less variable (< 1‰), and values are consistently more positive. The $\delta^{13}C$ plot shows that whilst there is less separation in the isotopic values of *Quinqueloculina* and *Ammonia* (compared to $\delta^{18}O$), values for *Quinqueloculina* show a much greater range of variation (+0.4 to −6.3‰). Values for *Ammonia* vary by < 1‰, and are generally more positive than *Quinqueloculina* above 8 ka, and more negative below this level. Two intervals marked by more strongly negative $\delta^{13}C$ ('M' peaks on Fig. 3) occur after 8 ka, and values for *Quinqueloculina* above 8 ka appear to be consistently more negative by at least 1‰ ('A' on Fig. 3). Previous work has shown that separation of the isotopic signatures of *Ammonia* and *Quinqueloculina* is likely a combination of vital effects and seasonal differences in the timing of shell calcification (Austin and Scourse, 1997; Scourse et al., 2002, 2004).

Whilst SEM images show no significant diagenetic carbonate overgrowths/infills of foraminifera, and excellent preservation (with submicron scale morphological detail and no conspicuous physical alteration of the skeletal micro-fabrics present), CL analysis revealed extensive luminescence (Fig. 9). Conventionally, luminescence is taken to signal diagenetic alteration, although it can also reflect variation in original environmental geochemistry influencing skeletal growth in foraminifera (Barbin, 2013). If diagenetic alteration is present, despite the seemingly exquisite preservation, then the broadly consistent pattern of variation between $\delta^{18}O$ and SST values (see Discussion; Fig. 3) suggests that it has not over-printed environmental signals, and that the broad trends shown by the stable isotope data are valid.

4.6. Rock-Eval

Organic matter (OM) in coastal and marine sediments may be characterised by hydrogen index (HI) values, which provide a measure of the extent of organic matter hydrogenation as well as an indication of pre- and post-depositional alteration effects (Lacey et al., 2014; Slowakiewicz et al., 2015). The HI profile for Borehole 89/15 suggests that the source of organic matter began to change after 8 ka (Fig. 3). The overall trend of increasing HI values after 8 ka suggests increasing amounts of marine/aquatic derived organic matter (Stephenson et al., 2005). The method of calculating HI, which is normalised to the Total Organic Content (TOC), means that unlike the latter, HI is unaffected by changes in sediment accumulation rate.

4.7. Sea surface temperatures (SST)

The results of alkenone-based SST estimates (Fig. 3) show that the interval 11.2–8.6 ka is characterised by values between 13.7 and 15.1 °C. Above this, there is a pronounced and sharply defined increase, with SST varying between 15.6 and 17.2 °C, continuing into the youngest analysed part of the succession.

The above SST estimates are comparable to the current (observed) summer SST values for the Irish Sea (Howarth, 2005), and are consistent with the current May and June blooming in the Irish Sea of haptophytes (Kennington and Rowlands, 2005), algae that include the source organisms of alkenones. These observations appear to suggest that $U^{K'}_{37}$ is recording summer SST in the Irish Sea. More generally, it has been suggested that the record of variation in $U^{K'}_{37}$ reflects the timing of the spring bloom and the intensity of this bloom compared to production throughout the rest of the year, with a significant summer bias in some settings (Jonas et al., 2017), particularly where environmental factors (e.g. insolation) limit winter productivity (Bachem et al., 2016).

5. Discussion

Comparison of the broad range of environmental proxy data assembled for this study (Fig. 3) reveals fundamental changes in microbiota, water temperature structure and sediment supply, allowing evaluation of the development, palaeoecological impact and long-term stability of seasonal stratification in the WIS. Today the WIS is a relatively deep water, open marine setting, characterised by a low-gradient salinity:$\delta^{18}O_{water}$ mixing-line (Austin et al., 2006, fig. 5), that in common with much of the north-west European shelf, allows the seasonal impact of changes in salinity on $\delta^{18}O_{water}$ to be ignored (Austin et al., 2006). Furthermore, the near ubiquitous presence of the remains

of echinoderms (almost exclusively stenohaline; Smith, 1984) in our calcareous micro-fossil sample residues, including cidarid echinoids from close to the base of the Holocene succession (39.15–39.17 m), suggests that normal salinity conditions have existed at the borehole site even at times of significantly lowered sea level. On this basis, the following discussion interprets changes in $\delta^{18}O$ values derived from benthic foraminifera as most probably reflecting changes in water temperature. Salinity effects may form components of anomalies on our stable isotope plots that are potentially associated with methane release and brine migration (see below), but these anomalies do not form part of the general trends in isotope data that we discuss. Furthermore, the impact of these potential brines is likely to be minor in terms of their stable isotope chemistry, and their ionic content significantly reduced by dilution.

5.1. Early Holocene (11.2–8.2 ka)

Two distinct environmental states are discernible in the Early Holocene record of the WIS: an early, 'high-productivity mixed water-mass state' (11.2–10 ka), and a later 'lower productivity mixed water-mass state' (10–8.2 ka) (Fig. 3). The first is characterised by a diverse assemblage of benthic foraminifera and ostracods (Dickson, 1995) and a predominance of heterotrophic dinoflagellate cysts (Figs. 3 and 6), reflected by D1 assemblage dinoflagellate cyst samples occupying a distinctly separate region of the DCA plot on Fig. 7. Abundant shelly macrofossils (e.g. oysters, cidarid echinoids) suggest relatively shallow, marine conditions, as do rare occurrences of the foraminifer *Elphidium macellum* and low relative abundances of *Spiniferites* and occasional high abundance of the coastal species *Votadinium calvum* (Zonneveld et al., 2013). Low dinoflagellate cyst concentrations (Fig. 3) are probably affected by very high sedimentation rate through this interval and relatively high tidal currents causing winnowing of silt-grade material. *Ammonia beccarii* is a highly adaptable and opportunistic species, surviving in regions affected by low oxygen levels, high inputs of nutrients and trace metals, and variable depth, temperature and salinity (Alve and Murray, 1999; Nikulina et al., 2008; Polovodova et al., 2009). Its sudden and short-lived abundance also at the base of the Holocene (F1 association) is probably an opportunistic response to a newly created habitat. Above this, *Pyrgo williamsoni* is a marker for the F2a assemblage, with two distinct abundance peaks (Fig. 4). This foraminifer is characteristic of shelfal environments (Murray, 2013), and in Arctic deglacial successions Cronin et al. (2017) assigned it to their "river-intermediate" assemblage (as distinct from "river proximal" and "river distal" associations) following Polyak et al. (2002). This ecological interpretation broadly fits with its occurrence in the WIS during the Early Holocene, when lowered sea level would have increased the impact of terrestrial sediment sources across the Irish Sea Basin (see below). The peaks in *P. williamsoni* may be related to changes in seabed conditions, as Novak (2017) reported a preference of this foraminifer for muddy substrates. If correct, these peaks potentially demonstrate cyclicity in the mud/sand ratio at the borehole site, and are possibly evidence of fine-scale lithological change in response to variation in the rate of sea level rise.

Summer SST values increase through the Early Holocene, peaking around 15 °C at 10.2 ka, and are mirrored by lower $\delta^{18}O$ values of benthic *Quinqueloculina*, suggesting that warming affected the whole water column and that the system was fully mixed. More generally, warming of the Early Holocene climate is marked across NW Europe by the rapid spread/appearance of hazel (*Corylus*) pollen (Tallantire, 2002; Theuerkauf et al., 2014), which in Borehole 89/15 was noted as reaching its acme in this interval. High sedimentation rates (1200–1600 cm/kyr) are associated with peak values in the Ti/K ratio, suggesting proportionately greater input of hydrodynamically heavy (i.e. coarse-grained) detrital sediment at this time. Although the concentrations of Rb are low, there is a suggestion in our Rb/K plot that the sediment deposited prior to 8 ka is geochemically contrasting to that deposited after 8 ka. Voluminous sediment supply, perhaps partly reflecting the availability of easily remobilised glacigenic sediment, could have boosted productivity through the supply of bio-limiting nutrients, explaining the abundance of heterotrophic dinoflagellate cysts and diverse and abundant benthic foraminifera. The high abundance of *Lingulodinium machaerophorum* in one sample could be interpreted as evidence for increased mixing (cf. Marret and Scourse, 2002) or is consistent with increased riverine input (e.g. Zonneveld et al., 2013).

Inferred lower sea-level (20–40 m below present level) across the Irish Sea basin during the Early Holocene (Stone et al., 2010; Smith et al., 2012), consistent with the dinoflagellate cyst record of this work, would have focused sedimentation towards the deeper WIS region, following a typical Low Stand Systems Tract pattern of deposition (Van Wagoner et al., 1988; Catuneanu et al., 2011). Amplification of this effect in the Irish Sea is likely to have been driven by: 1) unusual geometry of the Irish Sea basin, with a restricted deep water region to the west, and extensive, much shallower shelf to the east; 2) patterns of Early Holocene isostatic uplift across northern Britain that initially outpaced rates of sea-level rise (Smith et al., 2012), probably driving high sediment fluxes to adjoining depositional basins. In effect, the WIS basin probably acted as a sediment sink for material that was unable to be stored on the eastern shelf.

In the later part of the Early Holocene, a modest stepped phase of cooling in summer SSTs around 10 ka is matched by shifts to more positive $\delta^{18}O$ values of *Quinqueloculina*, marking the onset of a 'lower productivity mixed water state' (Fig. 3). The micro-biota is characterised by low diversity benthic foraminifera (particularly hyaline taxa) overwhelmingly dominated by *Quinqueloculina seminula*, lower abundances of heterotrophic dinoflagellate cysts and increasing dominance of the autotrophic genus *Spiniferites*. Compared to the D1 dinoflagellate cyst assemblage, samples comprising the D2 assemblage occupy a separate and non-overlapping region of the DCA plot, but have a broad spread, consistent with a shift to a distinctly different and/or more complex/rapidly varying environment. Coincident with this is a rise in Holocene sea-level, modest initially, culminating in a rapid phase of increase beginning around 8.8 ka (Fig. 3). The first appearance of *Operculodinium centrocarpum* sensu Wall and Dale (1966) and *S. membranaceus* represent an important shift in the dinoflagellate cyst record, reflecting a deeper environment with mostly mixed water conditions, and some influence of frontal zones (*S. quanta*, *S. ramosus*, cysts of *P. schwartzii*).

An interval dominated by *Quinqueloculina seminula* is recorded by Scourse et al. (2002) in the Holocene succession in the Celtic Sea between ca. 10.5 and 9 ka, interpreted to represent a high energy, shallow marine setting. This foraminifer is an active coloniser that is often associated with coarser-grained sediment substrates (Murray, 2006), and *Quinqueloculina* spp. in general show a preference for regions experiencing high velocity currents and low flux of organic carbon (Martins et al., 2006). Cearreta et al. (2002) also note that in settings where connections with oceanic waters are restricted, increasing that connectivity favours increasing abundance of *Q. seminula*.

Between 11 and 10 ka sediment accumulation rates are very high (ca. 1600–1200 cm/kyr) and are matched by peak values in Ti/K, before steadily declining. Ti/K values build again around 8 ka, although this is not matched by an increase in sedimentation rate. In situ sediment reworking is one possible explanation of the latter trend, although no complimentary macro-sedimentary features were noted in the core. Alternatively, rising concentration of Ti and declining sediment accumulation could indicate proportionately coarser sediment being moved across the borehole site because of lack of effective storage. This process of 'normal regression' (sensu Catuneanu et al., 2011) occurs when newly flooded basin margins are not initially able to store the sediment volumes they receive. In the eastern Irish Sea basin, this might also reflect strong tidal/storm scour, and possibly remobilisation of newly flooded and poorly consolidated sediment. This environment may have favoured the robust, heavily calcified *Quinqueloculina*, and perhaps

more generally the distinct shell calcification mechanism adopted by milliolid taxa which avoids the need for an organic template to control shell growth (de Nooijer et al., 2009).

The latest part of the Early Holocene (8.6 to 8.2 ka) in the WIS is marked by a dramatic warming of summer SST values, inferred to represent the establishment of seasonal stratification (see below). There is no evidence of the widely recognised globally cooler climate conditions around 8.2 ka, particularly affecting the North Atlantic region (Alley et al., 1997). Its absence in the WIS might be similar to other Atlantic sites where this event is undetected by SST data, possibly because of decoupling of surface and subsurface marine temperature records (Moros et al., 2004), or reflect the influence of local conditions (e.g. erosion/environmental over-printing) and/or low sample resolution.

5.2. Mid and Late Holocene (post 8.2 ka)

In the latest Early Holocene, the development of persistently higher average summer SST values coincides with a change from rapid to more gradually rising sea-level that continues through the Mid and Late Holocene (Fig. 3). Warming is not suggested by the $\delta^{18}O$ record of benthic *Quinqueloculina*, which (apart from some anomalously negative values; see below) generally shows a trend to more positive (i.e. cooler) values above the base of the Mid Holocene, at least until this foraminifer disappears from the WIS succession around 5.6 ka (Fig. 3). The Mid Holocene $\delta^{18}O$ record of *Quinqueloculina* with respect to *Ammonia* in the WIS is similar to the trend of these foraminifera from the Celtic Sea reported by Scourse et al. (2004). Austin and Scourse (1997) and Scourse et al. (2002, 2004) discussed seasonal differences in calcification that contribute (with vital effects) to an offset in the $\delta^{18}O$ records of *Quinqueloculina* and *Ammonia*. In this context, the apparent convergence of the trend of *Quinqueloculina* with the $\delta^{18}O$ record of *Ammonia* (Fig. 3) in both the Celtic Sea and WIS is plausible evidence for progressive reduction of this seasonal effect with the onset of stratification. Scourse et al. (2004) reported that in stratified settings, both *Ammonia* and *Quinqueloculina* select the same season (typically September) for calcification, when peak bottom water temperatures are achieved. The contrasting trends in SST and the $\delta^{18}O$ record of benthic *Quinqueloculina* described above and shown on Fig. 3 suggest the relatively rapid establishment of seasonal water-mass stratification around 8.4–8.2 ka that persists to the present day.

Negative shifts of $\delta^{13}C$ can also be used to recognise seasonal water-mass stratification, reflecting increased preservation of light organic carbon beneath the pycnocline (Austin and Scourse, 1997; Scourse et al., 2002, 2004). Understanding the $\delta^{13}C$ record for the WIS is complicated by some unusually negative values (see below), generally corresponding with intervals that also show abnormally negative $\delta^{18}O$. However, by considering only the difference between the maximum positive values of $\delta^{13}C$ for *Quinqueloculina* observed before and after the inflection in SST values ('A' on Fig. 3), there appears to be a small negative shift of about 1‰, similar to that associated with stratification in the Celtic Sea during the Holocene (Scourse et al., 2002). Large, short lived negative excursions in the $\delta^{13}C$ (> -6‰) and $\delta^{18}O$ data for *Quinqueloculina* ('M' on Fig. 3) depart significantly from the expected response to stratification (Austin and Scourse, 1997; Scourse et al., 2002). Geophysical data show the borehole site coincides with a significant area of shallowly-buried methane, with active seepage indicated by pockmarks (Crocker et al., 2005). By analogy with work elsewhere (Rathburn et al., 2003; Torres et al., 2003; Consolaro et al., 2015), the negative excursions in $\delta^{13}C$ (and presumably also $\delta^{18}O$) may document the influence of methane seeps in the WIS on the Mid and Late Holocene marine environment. The WIS material appears to show the typical variability of (amplified) negative $\delta^{13}C$ values within species and between species, indicative of a primary (and not diagenetic) signal, with marked disequilibrium with the strongly negative $\delta^{13}C$ of methane (Rathburn et al., 2003; Hill et al., 2004; Panieri et al., 2012; Consolaro et al., 2015). Temporal variability of methane seepage might explain the absence of isotope evidence for this feature in the Early Holocene, or the development of stratification could have boosted methane concentration in benthic settings by reducing turbulent mixing, a feature observed at North Sea methane seep sites (Mau et al., 2015).

Dinoflagellate cysts respond to the onset of stratification in the WIS by a progressive increase in the relative proportion of heterotrophic forms (especially *Brigantedinium* and *Votadinium*), and they largely dominate over autotrophic forms after 7.5 ka (Fig. 3), indicating greater primary productivity (Bringué et al., 2014). *Bitectatodinium tepikiense*, *Selenopemphix quanta* and *Spiniferites elongatus*, present in the D3 assemblage, associated with low abundance of *Spiniferites membranaceus*, characterise regions in the Celtic Sea associated with seasonal stratification, with *B. tepikiense* particularly favouring geographical regions where there is high seasonal temperature range (Marret et al., 2004). *Spiniferites lazus* was discussed extensively by Marret et al. (2004), who suggested that high relative abundances of this taxon might be related to warm temperatures and/or relatively lower sea level. In Borehole 89/15, this taxon builds to a peak of 30% abundance around the D2/D3 boundary, and then declines in abundance higher in the succession. Since the D2/D3 boundary is a time of rapidly rising sea level (Fig. 3), abundance of *S. lazus* might be a response to the onset of warmer surface water conditions created at the inception of seasonal stratification. Whilst potentially favourable for *S. lazus* initially, stabilisation of this higher productivity environment would have made it a niche with increasing competition and predation that might explain its subsequent progressive decline. Increasing influence of frontal conditions in the youngest part of the D3 succession (post-dating 3 ka), perhaps reflecting changing extent and pattern of the area of WIS seasonal stratification, is potentially signalled by increasing abundance of *S. ramosus* based on comparison with the Celtic Sea dinoflagellate cyst distributions (Marret et al., 2004).

The change in the character of the dinoflagellate cyst assemblage is clearly seen on the DCA plot, with D3 assemblage samples plotting between D1 and D2 samples, and younger samples in D3 tracking closer to the high productivity Early Holocene D1 assemblage. The persistent separation of the two high productivity assemblages on the DCA plot supports the view that these similar trophic strategies are a response to distinctly different environmental settings. The increase in heterotrophic cysts appears to track increasing HI. This, and the tendency in correspondence analysis (Fig. 7) for the youngest components of the D3 assemblage to track towards the D1 assemblage, suggests a trend of increasing productivity associated with increasing deposition of marine derived organic matter. This might indicate intensification of the thermocline during seasonal stratification (which in the WIS is sensitive to long-term variation in summer air temperatures and wind speeds; Olbert et al., 2011), or perhaps progressive growth in the nutrient content of water beneath the pycnocline as stratification became established; nutrients that amplify productivity at mixing fronts and across the Sub Chlorophyll Maximum, and contribute to increasing fluxes of heterotrophic cysts. However, the apparent stabilisation in the relative abundance of heterotrophic cysts after 5 ka probably shows that factors such as winter mixing and bioturbation (Austin and Scourse, 1997; Scourse et al., 2002, 2004) may ultimately limit the capacity of the WIS to progressively enhance the organic content of sediments through seasonal stratification.

Although numerically dominated by *Ammonia beccarii*, the F3 foraminiferal assemblage is uniquely distinguished by the record of *Spiroplectammina wrightii*, which appears to have a broad environmental tolerance, being recorded on sand and mud substrates in fully marine salinities (Murray, 1991 and references therein), and a component of both the mixed water assemblage (Scott et al., 2003, p. 46) as well as the fully stratified setting well away from frontal regions (ibidum, Appendix III) in the Celtic Sea. The relatively sudden appearance of this Mediterranean to Lusitanian species (Haynes, 1973, 1981) in the WIS around 8 ka, approximately coincident with the onset of seasonal

stratification, probably reflects a broader pattern of migration in response to improving marine conditions between the Early and Mid-Holocene (e.g. Andersson et al., 2010 and references therein). The F3 assemblage includes forms (*Nonionella turgida*, *Bulimina marginata*) that are characteristic of Recent sediments in the Celtic Sea associated with seasonal stratification and mixing fronts (Scott et al., 2003), with even low abundances of *N. turgida* (spiking at 18% in Borehole 89/15; Fig. 4) significant for interpretation of these environments (Scott et al., 2003).

The switch in the dominant benthic foraminifer, from *Quinqueloculina seminula* below the SST inflection, to *Ammonia beccarii* above, is remarkably sharp, and a feature seen in both absolute and relative abundance data (Fig. 4). *Quinqueloculina* spp. like *Ammonia* are opportunistic (Langlet et al., 2014 and references therein) with broad environmental tolerance, inhabiting lagoons, marshes and deeper inner shelf environments (Murray, 2006) with some ability to withstand low oxygen concentration (Langlet et al., 2014). Opportunistic behaviour of these taxa in Borehole 89/15 is suggested by the coincident peaks in absolute abundance at the approximate onset of seasonal stratification (Fig. 4). The subsequent decline in *Quinqueloculina* and dominance of *A. beccarii* suggests a pattern of environmental change that *Q. seminula* was less well adapted to over the longer term. The pattern of decline in *Q. seminula* is similar to that seen in the Celtic Sea (Austin and Scourse, 1997, fig. 5), but the dominance of *Ammonia* is distinctive of the WIS record. Experimental data suggests that *Q. seminula* is sensitive to prolonged deterioration in seabed oxygenation, although it might initially respond opportunistically if this is associated with greater availability of organic matter (Langlet et al., 2014), both factors associated with the onset of seasonal stratification in the Celtic Sea and WIS. The strongly contrasting record of *Ammonia* with respect to this event in the WIS suggests that it is responding to local environmental factors that favoured its abundance in the WIS following the onset of seasonal stratification. One possibility is that the WIS site provides a record of seasonal stratification that was sustained without interruption from the influence of a tidal mixing front. In the Celtic Sea, dinoflagellate cysts (Marret et al., 2004) provide some evidence for the migration of frontal conditions towards the site described by Austin and Scourse (1997) and Scourse et al. (2002). Alternatively, the presence of shallow-buried methane in the WIS may have tipped the ecological balance in favour of *Ammonia*, species of which are tolerant of a broad range of environmental disturbance (Alve and Murray, 1999; Nikulina et al., 2008; Polovodova et al., 2009; Gooday et al., 2009). This potentially includes a range of environmental factors associated with the presence of methane, for example hydrogen sulphide (noted on drilling logs of Borehole 89/15) and mineral-enriched fluids associated with gas emplacement (gypsum in the Holocene succession possibly remobilised from the thick underlying Permo-Triassic succession; Fig. 8). Although methane and associated fluid/gas release at the site is likely to have a long geological history in the WIS, the reduced water column mixing associated with seasonal stratification could have emphasised its ecological impact. Similarly, changes in sediment characteristics and diagenetic environment associated with the onset of stratification may explain why the upper limit of maximum gypsum concentration in Borehole 89/15 (Fig. 8) is approximately coincident with the horizon of SST inflection.

Since the current pattern of stratification in the WIS can be understood both in terms of water depth and low tidal energy (Howarth, 2005; Dabrowski et al., 2010), the significant rise in sea-level at the end of the Early Holocene was likely critical to establishing threshold values of these parameters for stratification to develop. Palaeotidal modelling (e.g. Scourse and Austin, 1995; Uehara et al., 2006; Ward et al., 2016) reconstructs the spatial and temporal changes of tidal dynamics through the Holocene for north-west European shelf seas, and can be used to predict the timing of onset of seasonal marine stratification. Using outputs from the Ward et al. (2016) palaeotidal simulations, the predicted timing for the onset of seasonal stratification at the site of Borehole 89/15 is around 10–9 ka, compared with the 8.4–8.2 ka indicated by this study. There are several reasons why these values might differ. Firstly, errors and assumptions in the age/depth model derived for Borehole 89/15 could cause differences between the modelled and observed timing of seasonal stratification. Secondly, palaeotidal models are highly sensitive to GIA effects (Uehara et al., 2006; Ward et al., 2016), and modelling of these in turn depends on assumptions on the rheology of the mantle and crust. Palaeotidal models are underpinned by an elastic density structure taken from an average-Earth seismic model by Dziewonski and Anderson (1981). This model uses a simple 3-layer earth model each with different viscosity values (Bradley et al., 2011), but Dziewonski and Anderson (1981) acknowledged that their average Earth Model does not take account of the very large lateral variations in the first few 10s km of the Earth's crust. New evidence for the crustal structure of the Irish Sea and wider north-west European region shows significant laterally heterogeneity, with fingers of low density rock radiating from a plume beneath Iceland; one such feature extends down the Irish Sea region (Schoonman et al., 2017, fig. 4). Bradley et al. (2011) refer to data-model misfit relating to “the lateral variations in earth properties”, shown to particularly affect Fennoscandia, which is also the site of one of the crustal anomalies identified by Schoonman et al. (2017). Until Earth models are developed that can fully reflect lateral and vertical heterogeneities in crustal structure, it is not possible to reach any firm conclusion about the source of misfit between modelled and observed data for the timing of marine stratification in the WIS area. Recent palaeotidal models of the region are dependent on a single ground-truth point in the Celtic Sea based on work by Austin and Scourse (1997) and Scourse et al. (2002) (Uehara et al., 2006; Neill et al., 2010; Ward et al., 2016), so in this context our data misfit with the timing of stratification predicted by palaeotidal models is potentially significant in providing a much-needed control point for validating/constraining palaeotidal model outputs.

As well as influencing marine stratification, rising sea-level through the Holocene also explains the sharp decline in sediment accumulation rate (to < 100 cm/kyr) in the Late Holocene. During high/maximum sea-level, detrital loads of riverine sources are easily trapped in the increased accommodation space at the basin margin. In the case of the Irish Sea Basin, small rises in sea-level across the expansive low relief of the eastern part of the basin would have added disproportionately to the capacity of this area to store sediment, evidenced by extensive modern sand and mud banks fringing the Lancashire coast. Higher residual sedimentation in the early part of the Mid Holocene (7.5–5.5 ka), and minor peaks between 6.1 and 5.8 ka (matched by peaks in Ti/K and Rb/K ratios) could reflect short-lived overspill from small infilled depocentres on the Eastern Irish Sea Shelf, before later Holocene sea-level rise created additional sediment-storage capacity across this region.

Although summer SST values are generally elevated in the WIS through the Mid and Late Holocene, there is a fluctuation between relatively warmer and cooler intervals. At least three of these fluctuations match warm/cold events recognised in the wider Northern Hemisphere Holocene climate (7.5, 4, and 3 ka; Wanner et al., 2014). The extent to which peaks in SST values in the WIS can be linked to solar variability is difficult to assess. Problems exist with the age calibration of different proxy data, but broadly, peaks in solar activity at 4.4 ka and 2.7 ka (Charman, 2010) correspond with times of elevated SST in the WIS. The sustained fall in summer SST values since 3 ka suggests a progressive weakening of the stratification in the WIS. This period includes significant cool phases and is part of a longer term, probably orbitally-driven Northern Hemisphere pre-industrial cooling trend, perhaps additionally influenced in the last 2000 years by groups of major volcanic eruptions, both acting to reduce summer insolation (Wanner et al., 2008; Charman, 2010; Wanner et al., 2014).

6. Conclusions

Seasonal stratification boosts modern day marine productivity in the WIS region, and based on the evidence of multi-proxy data from Borehole 89/15, became established around the transition from Early to Mid-Holocene (ca. 8.4–8.2 ka). This is slightly younger compared to the Celtic Sea (8.99 to 8.44 ka) but overlaps with palaeotidal model simulations of stratification onset (ca. 10–8 ka). In the WIS, seasonal stratification was preceded by two distinct Early Holocene mixed-water marine settings, a high productivity mixed water-mass state between 11.2 and 10 ka, and a period of lower productivity between 10 and 8.2 ka. In the Mid and Late Holocene (post 8.2 ka), rapid warming of summer SSTs (typically 16 to 17 °C) is associated with a trend of more positive $\delta^{18}O$ in benthic foraminiferal, suggesting a cooling of deeper water and the establishment of seasonal stratification. This change is associated with an increase in the burial of marine-derived organic matter (increasing HI) and long term increase and eventual dominance of heterotrophic dinoflagellate cysts.

The strong temporal association of increase in summer SSTs and maximum rate of sea-level rise suggests that threshold values in bathymetry and tidal energy are the main factors driving stratification in the WIS. Higher sediment supply to the WIS during lowered sea-level in the Early Holocene may have helped to sustain high productivity. Later rises in sea-level are associated with a decline in productivity and reduced sediment accumulation rate. Flooding and deepening across the eastern Irish Sea shelf likely increased the sediment storage potential of the shelf and restricted sediment fluxes to deeper regions westwards. Resurgence in WIS productivity occurred once sea-level rise was sufficient to allow seasonal stratification to become established. The effect of a reduction in turbulent mixing caused by stratification may have amplified the effects of local seabed methane seepage, by producing anomalously negative values of $\delta^{13}C/\delta^{18}O$ in benthic foraminifera and favouring the highly adaptable *Ammonia beccarii* as the dominant foraminifer species. Despite short term fluctuation in summer SSTs, after 8.2 ka there is no return to the values associated with the inferred mixed marine settings of the Early Holocene. A sustained decline in summer SSTs between ca. 3 ka and the end of our SST record at ca. 1.4 ka, suggests progressive weakening in the magnitude of the summer thermocline over this period.

Acknowledgements

We are grateful to Dr. Mike Ellis, BGS (Science Director Land, Soil & Coast programme) for supporting this research. ^{14}C dating was carried out by Dr. Mark Garnett, Natural Environment Research Council (NERC) Radiocarbon Facility (East Kilbride), UK, and Dr. Xiaomei Xu, University of California (Irvine), USA. We also thank Prof James Scourse (University of Exeter) for valuable dialogue and critical comment; Graham Lott (formerly BGS) for providing additional lithological details for Borehole 89/15, Simon Harris (BGS) for photography of core samples, Tim Heaton (BGS) for Sulphur isotope data, and Jeremy Rushton (BGS) for comments on SEM images of core material. All authors except De Schepper, Kender, Ward and Nichols publish with the approval of the Executive Director, British Geological Survey (NERC). SLW acknowledges NERC PhD studentship (NE/I527853/1).

Appendix A. Supplementary data

Supplementary data to this article can be found online at https://doi.org/10.1016/j.palaeo.2019.06.004.

References

Alley, R.B., Mayewski, P.A., Sowers, T., Stuiver, M., Taylor, K.C., Clark, P.U., 1997. Holocene climatic instability: a prominent, widespread event 8200 years ago. Geology 25, 483–486.

Alve, E., Murray, J.W., 1999. Marginal marine environments of the Skaerrak and Kattegat: a baseline study of living (stained) benthic foraminiferal ecology. Palaeogeogr. Palaeoclimatol. Palaeoecol. 146, 171–193.

Andersson, C., Pausata, F.S.R., Jansen, E., Risebrobakken, B., Telford, R.J., 2010. Holocene trends in the foraminifer record from the Norwegian Sea and the North Atlantic Ocean. Clim. Past 6, 179–193.

Ascough, P.L., Cook, G.T., Dugmore, A.J., Scott, E.M., 2005. Influence of mollusc species on marine ΔR determinations. Radiocarbon 47, 433–440.

Austin, W.E.N., Scourse, J.D., 1997. Evolution of seasonal stratification in the Celtic Sea during the Holocene. J. Geol. Soc. Lond. 154, 249–256.

Austin, W.E.N., Cage, A.G., Scourse, J.D., 2006. Mid-latitude shelf seas: a NW European perspective on the seasonal dynamics of temperature, salinity and oxygen isotopes. The Holocene 16, 937–947.

Bachem, P.E., Risebrobakken, B., De Schepper, S., McClymont, E.L., 2016. Highly variable Pliocene sea surface conditions in the Norwegian Sea. Clim. Past 13, 1153–1168.

Barbin, V., 2013. Application of cathodoluminesence microscopy to recent and past biological materials: a decade of progress. Mineral. Petrol. 107, 353–362.

Barker, S., Broecker, W., Clark, E., Hajdas, I., 2007. Radiocarbon age offsets of foraminifera resulting from differential dissolution and fragmentation within the sedimentary bioturbated zone. Paleoceanography 22, PA2205.

Blaauw, M., 2010. Methods and code for 'classical' age-modelling of radiocarbon sequences. Quat. Geochronol. 5, 512–518.

Bradley, S.L., Milne, G.A., Shennan, I., Edwards, R., 2011. An improved Glacial Isostatic Adjustment model for the British Isles. J. Quat. Sci. 26, 541–552.

Bringué, M., Pospelova, V., Field, D.B., 2014. High resolution sedimentary record of dinoflagellate cysts reflects decadal variability and 20th century warming in the Santa Barbara Basin. Quat. Sci. Rev. 105, 86–101.

Brooks, A.J., Bradley, S.L., Edwards, R.J., Milne, G.A., Horton, B., Shennan, I., 2008. Postglacial relative sea-level observations from Ireland and their role in glacial rebound modelling. J. Quat. Sci. 23, 175–192.

Butler, P.G., Scourse, J.D., Richardson, C.A., Wanamaker, A.D., 2009. Continuous marine radiocarbon reservoir calibration and ^{13}C Suess effect in the Irish Sea: results from the first multi-centennial shell-based marine master chronology. Earth Planet. Sci. Lett. 279, 230–241.

Catuneanu, O., Galloway, W.E., Kendall, C.G.St.C., Miall, A.D., Posamentier, H.W., Strasser, A., Tucker, M.A., 2011. Sequence stratigraphy: methodology and nomenclature. Newsl. Stratigr. 44, 173–245.

Cearreta, A., Alday, M., Freitas, C.M., Andrade, C., 2002. Modern foraminiferal record of alternating open and restricted environmental conditions in the Santo André lagoon, SW Portugal. Hydrobiologia 475/476, 21–27.

Chadwick, R.A., Jackson, D.I., Barnes, R.P., Kimbell, G.S., Johnson, H., Chiverell, R.C., Thomas, G.S.P., Jones, N.S., Riley, N.J., Pickett, E.A., Young, B., Holliday, D.W., Ball, D.F., Molyneux, S.G., Long, D., Power, G.M., Roberts, D.H., 2001. Geology of the Isle of Man and its offshore area. In: British Geological Survey Research Report RR/01/06.

Charman, D.J., 2010. Centennial climate variability in the British Isles during the mid – late Holocene. Quat. Sci. Rev. 29, 1539–1554.

Chesher, J.A., Wingfield, R.T.R., 1990. Shallow drilling programme Celtic and Irish seas 1989. Final Geological Report. British Geological Survey Technical ReportWB/90/2C.

Consolaro, C., Rasmussen, T.L., Panieri, G., Mienert, J., Bünz, S., Sztybor, K., 2015. Carbon isotope ($\delta^{13}C$) excursions suggest times of major methane release during the last 14 kyr in Fram Strait, the deep-water gateway to the Arctic. Clim. Past 11, 669–685.

Craig, H., 1957. Isotopic standards for carbon and oxygen and correction factors for mass spectrometric analysis. Geochemica et Cosmochemica Acta 12, 133–149.

Crocker, P.F., 1995. Shallow gas accumulation and migration in the western Irish Sea. Special Publication of the Geological Society, London 93, 41–58.

Crocker, P.F., Kozachenko, M., Wheeler, A.J., 2005. Gas-related seabed structures in the Western Irish Sea (IRL-SEA6). In: Technical Report produced for Strategic Environmental Assessment – SEA6. Petroleum Affairs Division, Ireland.

Cronin, T.M., O'Regan, M., Pearce, C., Genery, L., Toomey, M., Semiletov, I., Jakobsson, M., 2017. Deglacial sea level history of the East Siberian Sea and Chukchi Sea margins. Clim. Past 13, 1097–1110.

Dabrowski, T., Hartnett, M., Olbert, A.I., 2010. Influence of seasonal circulation on flushing of the Irish Sea. Mar. Pollut. Bull. 60, 748–758.

Dickson, C.P., 1995. Quaternary Ostracoda From the Celtic and Irish Seas: A Palaeoenvironmental Study (PhD Thesis). University of Wales, Aberystwyth.

Dziewonski, A.M., Anderson, D.L., 1981. Preliminary reference Earth model. Phys. Earth Planet. Inter. 25, 297–356.

Evans, G.L., Hardman-Mountford, N.J., Hartnoll, R.G., Kennington, K., Mitchelson-Jacob, E.G., Shammon, T., Williams, P.J. le B., 2003. Long-term environmental studies in the Irish Sea: a review. In: Scientific Report No. 2, (Marine Environmental Change Network, DEFRA 11/03).

Gooday, A.J., Jorissen, F., Levin, L.A., Middelburg, J.J., Naqvi, S.W.A., Rabalais, N.N., Scranton, M., Zhang, J., 2009. Historical records of coastal eutrophication-induced hypoxia. Biogeosciences 6, 1707–1745.

Gowen, R.J., McCullough, G., Dickey-Collas, M., Kleppel, G.S., 1998. Copepod abundance in the western Irish Sea: relationship to physical regime, phytoplankton production and standing stock. J. Plankton Res. 20, 315–330.

Greenwood, N., Parker, E.R., Fernand, L., 2010. Detection of low bottom water oxygen concentrations in the North Sea; implications for monitoring and assessment of ecosystem health. Biogeosciences 7, 1357–1373.

Haynes, J.R., 1973. Cardigan Bay recent foraminifera. Bulletin of the British Museum (Natural History) 4, 126–143 Zoology Supplement.

Haynes, J.R., 1981. Foraminifera. Macmillan Publishers Ltd., London.

Heier-Nielsen, S., Conradsen, K., Heinemeier, J., Knudsen, K.L., 1995. Radiocarbon dating of shells and foraminifera from the Skagen core, Denmark: evidence for reworking. Radiocarbon 37, 119–130.
Hill, A.E., Brown, J., Fernand, L., 1996. The western Irish Sea gyre: a retention system for Norway lobster (*Nephrops norvegicus*)? Oceanol. Acta 19, 357–368.
Hill, T.M., Kennett, J.P., Valentine, D.L., 2004. Isotopic evidence for the incorporation of methane-derived carbon into foraminifera from modern methane seeps, Hydrate Ridge, Northeast Pacific. Geochimica et Cosmochimica 68, 4619–4627.
Howarth, M.J., 2005. Hydrography of the Irish Sea. (SEA6 Technical Report, UK Department of Trade and Industry offshore energy Strategic Environmental Assessment programme. POL Internal Document 174: 30 p).
Jackson, D.I., Jackson, A.A., Evans, D., Barnes, R.P., Arthur, M.J., Howells, M.F., Hughes, R.A., Petterson, M.G., 1995. The Geology of the Irish Sea. United Kingdom Offshore Regional Report HMSO for the British Geological Survey, London.
Jonas, A.–.S., Schwark, L., Bauersachs, T., 2017. Late Quaternary water temperature variations of the Northwest Pacific based on the lipid paleothermometers TEX_{86}^{H}, $U^{K'}_{37}$ and LDI. Deep-Sea Res. 125, 81–93.
Judd, A.G., 2005. The distribution and extent of methane-derived authigenic carbonate. DTI Strategic Environmental Assessment 6 (SEA6) Area.
Kennington, K., Rowlands, W.L.l., 2005. Plankton Ecology of the Irish Sea. SEA6 Technical Report UK Department of Trade and Industry offshore energy Strategic Environmental Assessment programme. (61 p.).
Lacey, J.H., Francke, A., Leng, M.J., Vane, M.J., Wagner, B., 2014. A high-resolution Late Glacial to Holocene record of environmental change in the Mediterranean from Lake Ohrid (Macedonia/Albania). Int. J. Earth Sci. 104, 1–16.
Lambeck, K., 1995. Late Devensian and Holocene shorelines of the British Isles and North Sea from models of glacio-hydro-isostatic rebound. J. Geol. Soc. Lond. 152, 437–448.
Lambeck, K., Purcell, A.P., 2001. Sea-level change in the Irish Sea since the Last Glacial Maximum: constraints from isostatic modelling. J. Quat. Sci. 16, 497–506.
Langlet, D., Baal, C., Geslin, E., 2014. Foraminiferal species responses to in situ experimentally induced anoxia in the Adriatic Sea. Biogeosci. Discuss. 11, 1775–1797.
Marret, F., Scourse, J., 2002. Control of modern dinoflagellate cyst distribution in the Irish and Celtic seas by seasonal stratification dynamics. Mar. Micropaleontol. 47, 101–116.
Marret, F., Scourse, J., Austin, W., 2004. Holocene shelf-sea seasonal stratification dynamics: a dinoflagellate cyst record from the Celtic Sea, NW European Shelf. The Holocene 14, 689–696.
Martins, V., Jouanneau, J.-M., Weber, O., Rocha, F., 2006. Tracing the late Holocene evolution of the NW Iberian upwelling system. Marine Micropalaeontology 59, 35–55.
Mau, S., Gentz, T., Körber, J.-H., Torres, M.E., Römer, M., Sahling, H., Wintersteller, P., Martinez, R., Schlüter, M., Helmke, E., 2015. Seasonal methane accumulation and release from a gas emission site in the central North Sea. Biogeosciences 12, 5261–5276.
Moros, M., Emeis, K., Risebrobakken, B., Snowball, I., Kuijpers, A., McManus, J., Jansen, E., 2004. Sea surface temperatures and ice rafting in the Holocene North Atlantic: climate influences on northern Europe and Greenland. Quat. Sci. Rev. 23, 2113–2126.
Müller, P.J., Kirst, G., Ruhland, G., Von Storch, I., Rosell-Melé, A., 1998. Calibration of the alkenone paleotemperature index (UK′37) based on core tops from the eastern South Atlantic and the global ocean (60°N–60°S). Geochim. Cosmochim. Acta 62, 1757–1772.
Murray, J.W., 1971. An Atlas of British Recent Foraminiferids. Heinemann Educational Books, London.
Murray, J.W., 1973. Distribution and Ecology of Living Benthic Foraminiferids. Heinemann Educational Books, London.
Murray, J.W., 1991. Ecology and Palaeoecology of Benthic Foraminifera. Longman Scientific & Technical, Harlow.
Murray, J.W., 2006. Ecology and applications of Benthic foraminifera. Cambridge University Press, Cambridge.
Murray, J.W., 2013. Living benthic foraminifera: biogeographical distributions and the significance of rare morphospecies. J. Micropalaeontol. 32, 1–58.
Neill, S.P., Scourse, J.D., Uehara, K., 2010. Evolution of bed shear stress distribution over the northwest European shelf seas during the last 12 000 years. Ocean Dyn. 60, 1139–1156.
Nikulina, A., Polovodova, I., Schönfeld, J., 2008. Foraminiferal response to environmental changes in Kiel Fjord, SW Baltic Sea. eEarth 3, 37–49.
de Nooijer, L.J., Toyofuku, T., Kitazato, H., 2009. Foraminifera promote calcification by elevating their intracellular pH. PNAS 106, 15374–15378.
Novak, J.D., 2017. Holocene Palaeoenvironmental Reconstruction in Galway Bay, a Shallow Coastal Embayment Along Ireland's North-east Atlantic Margin (Unpublished PhD thesis). University of Limerick.
Olbert, A.I., Hartnett, M., Dabrowski, T., Mikolajewicz, U., 2011. Long-term inter-annual variability of a cyclonic gyre in the western Irish Sea. Cont. Shelf Res. 31, 1343–1356.
Panieri, G., Camerlenghi, A., Cacho, I., Cervera, C.S., 2012. Tracing seafloor methane emissions with benthic foraminifera: results from the Ana submarine landslide (Eivissa Channel, Western Mediterranean Sea). Mar. Geol. 291-294, 97–112.
Polovodova, I., Nikulina, A., Schönfeld, J., 2009. Recent benthic foraminifera in the Flensburg Fjord (Western Baltic Sea). J. Micropalaeontol. 28, 131–142.
Polyak, L., Korsun, S., Febo, L., Stanovoy, V., 2002. Benthic foraminiferal assemblages from the southern Kara Sea, a river-influenced arctic marine environment. J. Foraminifer. Res. 32, 252–273.
Prahl, F.G., Wakeham, S.G., 1987. Calibration of unsaturation patterns in long-chain ketone compositions for palaeotemperature assessment. Nature 330, 367–369.
Rathburn, A.E., Pérez, M.E., Martin, J.B., 2003. Relationships between the distribution and stable isotopic composition of living benthic foraminifera and cold methane seep biogeochemistry in Monterey Bay, California. Geochem. Geophys. Geosyst. 4, 1106.
Riding, J.B., 1995. A palynological investigation of fourteen samples from BGS borehole 89/15, 5.00 m to 45.00 m. British Geological Survey Technical Report WH/95/36C.
Rippeth, T.P., 2005. Mixing in seasonally stratified shelf seas: a shifting paradigm. Philosophical Transactions of the Royal Society, Series A 363, 2837–2854.
Roberts, D.H., Chiverrell, R.C., Innes, J.B., 2006. Holocene sea levels, Last Glacial Maximum glaciomarine environments and geophysical models in the northern Irish Sea Basin, UK. Mar. Geol. 231, 113–128.
Schoonman, C.M., White, N.J., Pritchard, D., 2017. Radial viscous fingering of hot asthenosphere within the Icelandic plume beneath the North Atlantic Ocean. Earth Planet. Sci. Lett. 468, 51–61.
Scott, G.A., Scourse, J.D., Austin, W.E.N., 2003. The distribution of benthic foraminifera in the Celtic Sea: the significance of seasonal stratification. J. Foraminifer. Res. 33, 32–61.
Scourse, J.D., Austin, W.E.N., 1995. Palaeotidal modelling of continental shelves: marine implications of a land-bridge in the Strait of Dover during the Holocene and middle Pleistocene. In: Preece, R.C. (Ed.), Island Britain: a Quaternary perspective. 96. Geological Society of London, Special Publication, pp. 75–88.
Scourse, J.D., Austin, W.D., Long, B.T., Assinder, D.J., Huws, D., 2002. Holocene evolution of seasonal stratification in the Celtic Sea: refined age model, mixing depths and foraminiferal stratigraphy. Mar. Geol. 191, 119–145.
Scourse, J.D., Kennedy, H., Scott, G.A., Austin, W.E.N., 2004. Stable isotopic analyses of modern benthic foraminifera from seasonally stratified shelf seas: disequilibria and the 'seasonal effect'. The Holocene 14, 747–758.
Sharples, J., 2008. Potential impacts of the spring-neap tidal cycle on shelf sea primary production. J. Plankton Res. 30, 183–197.
Sharples, J., Holt, J., Dye, S., 2010. Shelf Sea Salinity in MCCIP Annual Report Card 2010-11. MCCIP Science Review. 6pp. www.mccip.org.uk/arc.
Shennan, I., Horton, B., 2002. Holocene land-and sea-level changes in Great Britain. J. Quat. Sci. 17, 511–526.
Slowakiewicz, M., Tucker, M.E., Vane, C.H., Harding, R., Collins, A., Pancost, R.D., 2015. Shale-gas potential of the mid-Carboniferous Bowland-Hodder unit in the Cleveland Basin (Yorkshire), Central Britain. J. Pet. Geol. 38, 59–76.
Smith, A.B., 1984. Echinoid Palaeobiology. George Allen & Unwin, London.
Smith, D.E., Hunt, N., Firth, C.R., Jordan, J.T., Fretwell, P.T., Harman, M., Murdy, J., Orford, J.D., Burnside, N.G., 2012. Patterns of relative sea level change in the North of Britain and Ireland. Quat. Sci. Rev. 54, 58–76.
Stephenson, M.H., Leng, M.J., Vane, C.H., Osterloff, P., 2005. Investigating the record of Permian climate change from argillaceous sedimentary rocks, Oman. J. Geol. Soc. 162, 641–651.
Stone, P., Millward, D., Young, B., Merritt, J.W., Clarke, J.W., McCormac, S.M., Lawrence, D.J., 2010. British Regional Geology: Northern England, fifth edition. British Geological Survey, Keyworth, Nottingham.
Tallantire, P.A., 2002. The early-Holocene spread of hazel (*Corylus avellana* L.) in Europe north and west of the Alps: an ecological hypothesis. The Holocene 12, 81–96.
Theuerkauf, M., Bos, J.A.A., Jahns, S., Janke, W., Kuparinen, A., Stebich, M., Joosten, H., 2014. *Corylus* expansion and persistent openness in the early Holocene vegetation of northern central Europe. Quat. Sci. Rev. 90, 183–198.
Torres, M.E.M., Mix, A.C., Kinports, K., Haley, B., 2003. Is methane venting at the seafloor recorded by $\delta^{13}C$ of benthic foraminifera shells? Paleoceanography 18, 1062.
Uehara, K., Scourse, J.D., Horsburgh, K.J., Lambeck, K., Purcell, A.P., 2006. Tidal evolution of the north-west European shelf seas from the Last Glacial maximum to the present. J. Geophys. Res. 111, C09025.
Van Wagoner, J.C., Posamentier, H.W., Mitchem, R.M., Vail, P.R., Sarg, J.F., Loutit, T.S., Hardenbol, J., 1988. An overview of the fundamentals of sequence stratigraphy and key definitions. SEPM Spec. Publ. 42, 39–45.
Walker, M.J.C., Berkelhammer, M., Björck, S., Cwynar, L.C., Fisher, D.A., Long, A.J., Lowe, J.J., Newnham, R.M., Rasmussen, S.O., Weiss, H., 2012. Formal subdivision of the Holocene Series/Epoch: a discussion paper by a Working Group of INTIMATE (Integration of ice-core, marine and terrestrial records) and the Subcommission on Quaternary Stratigraphy (International Commission on Stratigraphy). J. Quat. Sci. 27, 649–659.
Walker, M., Head, M.J., Berkelhammer, M., Björck, S., Cheng, H., Cwynar, L., Fisher, D., Gkinis, V., Long, A., Lowe, J., Newnham, R., Rasmussen, S.L., Weiss, H., 2018. Formal ratification of the subdivision of the Holocene Series/Epoch (Quaternary system/period): two new Global Boundary Stratotype Sections and Points (GSSPs) and three new stages/subseries. Episodes 41, 213–223.
Wall, D., Dale, B., 1966. "Living fossils" in western Atlantic plankton. Nature 211, 1025–1026.
Wanner, H., Beer, J., Bütikofer, J., Crowley, T.J., Cubasch, U., Flückiger, J., Goosse, H., Grosjean, M., Joos, F., Kaplan, J.O., Küttel, M., Müller, S.A., Prentice, I.C., Solomina, O., Stocker, T.F., Tarasov, P., Wagner, M., Widmann, M., 2008. Mid- to Late Holocene climate change: an overview. Quat. Sci. Rev. 27, 1791–1828.
Wanner, H., Mercolli, L., Grosjean, M., Ritz, S.P., 2014. Holocene climate variability and change; a data-based review. J. Geol. Soc. Lond. 172, 254–263.
Ward, S.L., Neill, S.P., Scourse, J.D., Bradley, S.L., Uehara, K., 2016. Sensitivity of palaeotidal models of the northwest European shelf seas to glacial isostatic adjustment since the Last Glacial Maximum. Quat. Sci. Rev. 151, 198–211.
Wilkinson, I.P., 1995. Post-glacial and Holocene foraminifera from borehole 89/15, Irish Sea. British Geological Survey Technical Report WH/95/75C.
Williams, C., Sharples, J., Green, M., Mahaffey, C., Rippeth, T., 2013. The maintenance of the subsurface chlorophyll maximum in the stratified western Irish Sea. Limnology and Oceanography: Fluids & Environments 3, 61–73.
Williams, G.L., Fensome, R.A., MacRae, R.A., 2017. The New Lentin and Williams Index 2017. AASP Contribution Series 48, 1–1097.
Winckler, G., Aeschbach-Hertig, W., Holocher, J., Kipfer, R., Levin, I., Poss, C., Rehder, G.,

Suess, E., Schlosser, P., 2002. Noble gases and radiocarbon in natural gas hydrates. Geophys. Res. Lett. 29, GL014013.
Wollast, R., 1998. Evaluation and comparison of the global carbon cycle in the coastal zone and in the open ocean. In: Brink, K.H., Robinson, A.R. (Eds.), The Sea - The Global Coastal Ocean: Ideas and Observations on Progress in the Study of the Seas. 10. pp. 213–252.
Wood, G.D., Gabriel, A.M., Lawson, J.C., 1996. Palynological techniques – processing and microscopy. American Association of Stratigraphic Palynologists Foundation Dallas 1, 29–50.
Yagasaki, K., Ashi, J., Yokoyama, Y., Miyairi, Y., Kuramoto, S., 2016. Analysis of past recurrent methane seep activity using radiocarbon dating of *Calyptogena* spp. Shells in the eastern Nankai subduction zone, Japan. Geophysical Research Abstracts 18, EGU2016–3391-1.
Zonneveld, K.A.F., Marret, F., Versteegh, G.J.M., Bogus, K., Bonnet, S., Bouimetarhan, I., Crouch, E., de Vernal, A., Elshanawany, R., Edwards, L., Esper, O., Forke, S., Grøsfjeld, K., Henri, M., Holzwarth, U., Kielt, J.-F., Kim, S.-Y., Ladouceur, S., Ledu, D., Chen, L., Limoges, A., Londeix, L., Lu, S.-H., Mahmoud, M.S., Marino, G., Matsuoka, K., Matthiessen, J., Mildenhal, D.C., Mudie, P., Neil, H.L., Pospelova, V., Qi, Y., Radi, T., Richerol, T., Rochon, A., Sangiorgi, F., Solignac, S., Turon, J.-L., Verleye, T., Wang, Y., Wang, Z., Young, M., 2013. Atlas of modern dinoflagellate cyst distribution based on 2405 data points. Rev. Palaeobot. Palynol. 191 (1–197).